Ph.D DISSERTATION

A STUDY ON WIRELESS LOW POWER TRANSCEIVER FOR MEDICAL IMPLANT APPLICATION

의료용 인체 삽입물을 위한 무선 저전력 송수신기에 관한 연구

BY
KIHYUN KIM

FEBRUARY 2016

SCHOOL OF ELECTRICAL ENGINEERING AND
COMPUTER SCIENCE COLLEGE OF ENEGINEEING
SEOUL NATIONAL UNIVERSITY

공학박사 학위논문

A STUDY ON WIRELESS LOW POWER TRANSCEIVER FOR MEDICAL IMPLANT APPLICATION

의료용 인체 삽입물을 위한 무선 저전력 송수신기에 관한 연구

2016년 2월

서울대학교 대학원

전기·컴퓨터 공학부

김 기 현

Abstract

This thesis presents the wireless transceiver for medical implant application. The high propagation loss in human body which has high relative permittivity and conductive makes the implantable device be required for high sensitivity. Moreover, the device should have low power consumption to use for wireless implant medical application due to a restricted battery life. Also, this problem should be solved for on-body device considering integration with mobile device in the future. Simultaneously, the specific medical application such as epiretinal prosthesis, multi-channel electroencephalogram sensor demand high-data rate. Therefore, it is a main challenge that enhancing the device's power consumption and data-rate for implantable medical application. In order to enhance the performance of the device, several techniques are proposed in implantable human body transceivers.

Firstly, the propagation loss in human-body is calculated for determine the frequency for medical implant application. The frequency bands allocated by FCC or MICS are too narrow and high lossy bands in human-body. For this reason, the optimum frequency for Implantable medical device is found by using Friss's formula and the link budget is calculated for capsule endoscopy system. The optimum frequency is verified through image recovery experiment in liquid human phantom and pig by using designed capsule endoscopy system.

Secondly, the Super-Regenerative Receiver (SRR) with Digital Self-Quenching Loop (DSQL) is proposed for low power consumption. The proposed DSQL replaces the envelope detector used in a conventional SRR and minimizes power consumption by generating a self-quench signal digitally for a super-regenerative oscillator. The measurement results are given to show the performance of the proposed receiver.

Thirdly, the RF Current Reused and Current Combining (CRCC) Power Amplifier (PA) is proposed for low power and high-speed transmitter. Normally, the PA having low output power has a feasibility issue that an optimum impedance of PA is too high to match with antenna impedance. For this reason, obtaining the maximum efficiency of PA is difficult for conventional structure. Moreover, conventional PA's output bandwidth is to be narrow due to high impedance transform ratio between PA's output and antenna's input impedances. The CRCC structure solves this issue by decreasing the impedance transform ratio. The transmitter with CRCC PA is designed and verified through the measurement.

Keywords: capsule endoscopy transceiver, current combining, current reuse, low power, medical implant, OOK modulation, super regenerative, self-quench, high efficiency, high speed.

Student number: 2010-30975

Contents

Abstract ..... **i**

Contents ..... **iii**

List of Figures ..... **vi**

List of Tables ..... **x**

1. Introduction **1**

1.1 WBAN (Wireless Body Area Network) 1

1.2 Challenges in Designing Transceiver for Medical Implant Application 7

2. Propagation Loss in Human Body **10**

2.1 Introduction 10

2.2 Far field approximation in human-body 13

2.3 Calculation of propagation loss in human-body 15

2.3.1 Friss's formula 15

2.3.2 Efficiency of transmitting antenna in human-body 17

2.4 Calculation of propagation loss in human-body and conclusion 19

3. A Design of Transceiver for Capsule Endoscopy Application 21

3.1 Introduction 21

3.2 System Link Budget Calculation 24

3.3 Implementation 26

3.3.1 Transmitter with class B amplifier. 26

3.3.2 Super-heterodyne receiver with AGC. 28

3.3.3 Measurement results 30

3.4 Image recovery experiment 35

3.4.1 Integration of capsule endoscopy. 35

3.4.2 Image recovery in the liquid human phantom 38

3.4.3 Image recovery in a pig's stomach and large intestine. 40

3.5 Conclusion 41

4. Super-Regenerative Receiver with Digitally Self-Quenching Loop 42

4.1 Introduction 42

4.1.1 Selection of receiver's architecture for implantable medical device 44

4.1.2 Previous study of super-regenerative receiver 50

4.2 Main idea of proposed super-regenerative receiver 51

4.3 Description of proposed receiver 53

4.3.1 Digital self-quenching loop 55

4.3.2 Low noise amplifier and super-regenerative oscillator 57

4.3.3 Active RC filter for low power consumption 59

4.4 Experimental results 63

4.5 Summary and conclusion 69

5. A Transmitter with Current-Reused and Current-Combining PA 71

5.1 Introduction 71

5.1.1 Previous study of OOK transmitter 72

5.2 Main idea of proposed transmitter 73

5.3 Description of proposed transmitter 79

5.3.1 Current-combining and current-reused PA 79

5.3.2 Ring oscillator with driving buffer 83

5.4 Experimental Results 85

5.5 Summary and conclusion 93

6. Conclusion 95

7. Appendix 97

7.1 Output spectrum of OOK signal 97

7.2 Theoretical BER of OOK comunication 99

List of Figures

Fig. 1.1 Wireless Body Area Network 2

Fig. 1.2 Endoscopy capsule system with human body model. 4

Fig. 1.3 System overview of an epiretinal prosthesis. 5

Fig. 1.4 Change of future medical services with WBAN. 6

Fig. 2.1 Conceptual figure in propagation loss calculation. 16

Fig. 2.2 Calculated propagation loss in human-body. 20

Fig. 3.1 OOK transmitter for a capsule endoscopy. 26

Fig. 3.2 Super-heterodyne receiver with AGC for a capsule endoscopy. 28

Fig. 3.3 Microphotograph of designed system: transmitter and receiver. 30

Fig. 3.4 The transmitter measurement results : (a) output spectrum (b) average channel power in 20 MHz. 31

Fig. 3.5 Small signal gain of LNA with SAW filter at vector network analyzer. 33

Fig. 3.6 Bit-Error-Rate test results at Agilent E4438C. 34

Fig. 3.7 Photo of the integrated capsule endoscopy. 37

Fig. 3.8 Connection between balun and antenna 37

Fig. 3.9 Image recovery test in the liquid human phantom: (a) Measurement setup (b) Actual object (left) and captured image (right) 39

Fig. 3.10 Image recovery test in the aliving pig : (a) stomach wall and (b) large intestine wall. 40
Fig. 4.1 Wireless telemetry system for healthcare application. 43
Fig. 4.2 Block diagram of super-heterodyne receiver 44
Fig. 4.3 Block diagram of a direct-conversion receiver 45
Fig. 4.4 Block diagram of a super-regenerative receiver. 47
Fig. 4.5 Concept of a super-regenerative receiver. 47
Fig. 4.6 Average power consumption of the proposed receiver and a conventional SRR receiver. 51
Fig. 4.7 Block diagram of proposed receiver. 54
Fig. 4.8 Operation of proposed receiver at time-domain 54
Fig. 4.9 Gate level schematic of the digital self-quenching loop 55
Fig. 4.10 Schematic of a LNA with a matching network and a SRO with a differential buffer. 57
Fig. 4.11 Schematic of the active RC filter. 59
Fig. 4.12 Simulation result of LNA stage. 61
Fig. 4.13 Transient simulation of proposed receiver 62
Fig. 4.14 S (1, 1) of proposed receiver 63
Fig. 4.15 Measured frequency variation of quench signal Q(t) in time-domain : (a) without RF input signal and (b) with -70 dBm RF input signal 64

Fig. 4.16 Measured demodulated data, quench, and RF input signals at 10 Mbps in a time-domain 65
Fig. 4.17 Measured demodulated data (up) with original data (down) at 5 Mbps, -83 dBm 65
Fig. 4.18 BER measurement results of the designed receiver. 67
Fig. 4.19 Total energy consumption for the receiver at each data rates. A chip photo of the proposed receiver is also shown 68
Fig. 5.1 LC matching network for impedance transform 74
Fig. 5.2 Block diagram of the OOK transmitter with proposed PA 75
Fig. 5.3 Example for comparing conventional PA with proposed PA 77
Fig. 5.4 Schematics of proposed PA comprised of two amplifier units 80
Fig. 5.5 Load line graphs of conventional and proposed PAs 82
Fig. 5.6 Schematic of ring oscillator with driving buffer 84
Fig. 5.7 Simulated time period of ring oscillator from start-up to steady state 84
Fig. 5.8 Measured drain efficiency and output power of proposed power amplifier. A chip photo of the designed transmitter is also shown 86
Fig. 5.9 Measured output spectrum of PA under the continuous power state (a) and modulated power state (b) with 100 Mbps data-rate of PRBS pattern 88
Fig. 5.10 Measured time-domain output signal of transmitter with ‘1010’ data at 100 Mbps 89

Fig. 5.11 Measured frequency drift of proposed transmitter..... 89

Fig. 5.12 Measured efficiency and average output power, energy usage of transmitter at each data rates with PRBS pattern. 91

Fig. 5.13 ADS simulation results at gate with modulated signal 91

Fig. 5.14 Measured time-domain signal at transmitter's output with PRBS data (100 Mbps) 92

Fig. 7.1 Simulated output spectrum of transmitter (a) and measure output spectrum of transmitter with 100 Mbps data-rate of '1010' pattern 98

Fig. 7.2 Calculated results of theoretical BER of OOK communication 100

List of Tables

TABLE 2.1 Human-body model in FCC 11

TABLE 2.2 Calculated results of wave-length in human-body (muscle) 14

TABLE 3.1 Link budget of OOK system for a wireless capsule endoscope 25

TABLE 3.2 Feature of designed transmitter for a wireless capsule endoscope 32

TABLE 3.3 Feature of designed receiver of a wireless capsule endoscope 34

TABLE 4.1 Comparison of different receiver architectures 49

TABLE 4.2 Comparison with a recent super-regenerative receiver 70

TABLE 5.1 Comparison with OOK transmitter 94

Chapter 1

Introduction

1.1 Wireless Body Area Network (WBAN)

A wireless communication and devices have been developed for improving quality of our life. The size of device is minimized enough to be held by our single hand. Having mobile devices, we can access the internet anytime in everywhere. It is evitable that many things in our life will be united with internet and can be controlled by touching one button in the future.

In aspect of medical application, the people interest health care technology due to aging population. For the health examination, the patient should go to hospital to be diagnosed. It usually spends much time to test the health medical examination. This makes people be uncomfortable and inconvenient, especially for the senior

citizen. Therefore, the requirement for simplified process during the health examination and comfortable diagnosis technique is demanded.

Using WBAN (Wireless Body Area Network), the various diagnosis techniques have been proposed to provide people to comfortable and convenient process. The WBAN is a wireless network of wearable or implantable with embedded computing devices. The advance of low power integrated circuits, physiological sensors, small antenna and battery have miniaturized the whole system enough to be attached or be implanted to a human body. The WBAN give us cost effective and continuous health monitoring using biosensor. The gathered medical records are utilized for diagnosing patient and monitored with real-time through the wireless communication [1]-[4].

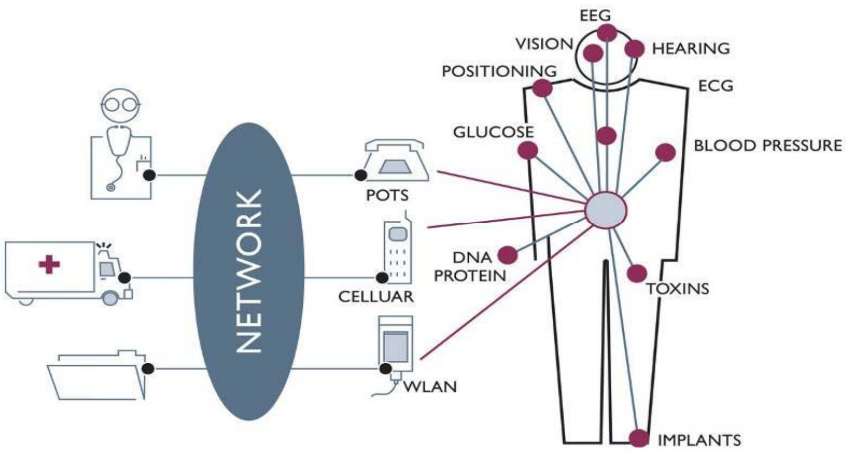

Fig. 1.1 Wireless Body Area Network [5]

One of the applications using WBAN is capsule endoscopy. An endoscope is an essential device in medical applications for its ability to examine the digestive tract accurately. However, it is inconvenient to use in a conventional wired endoscopy system because wired endoscopy causes considerable discomfort to patients. Also, the conventional instrument is limited in terms of its test coverage due to its finite length. Moreover, in the long and twisted small intestine, it is cannot easily access all of the digestive organs. These issues are directly related to the reliability of the diagnosis. The wireless capsule system whom Iddan was the first to describe is suitable for a substitution device of conventional endoscopy [6]. It could be small enough to be swallowed by patients without causing any discomfort. And, the capsule system has the advantage of offering a means of direct examination of the entire digestive tract with no anesthesia or insufflations. Therefore, many systems for Radio Frequency (RF) capsule endoscopy have been developed in the 433/868/915 bands or 2.4 GHz bands [7], [8].

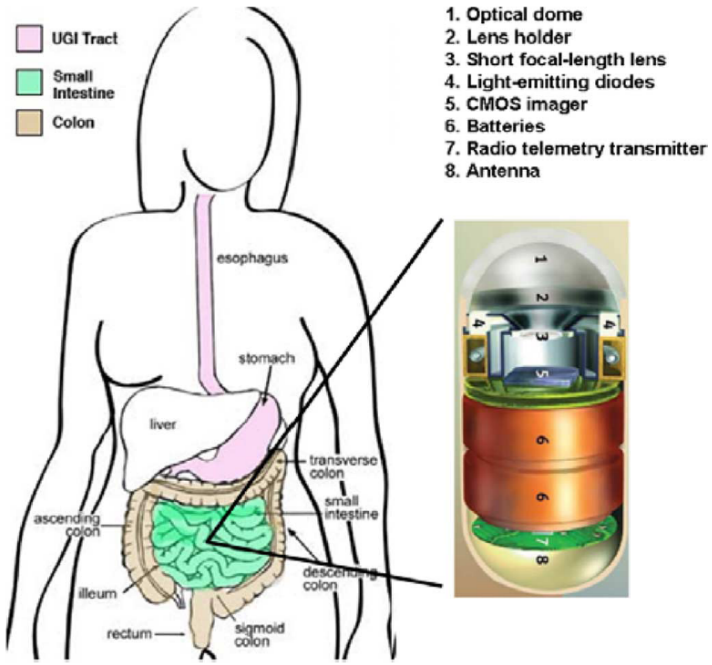

Fig. 1.2 Endoscopy capsule system with human body model [9]

Also, there are other applications using WBAN. Over the decades, visual prostheses based on functional electrical stimulation (FES) have been brought to great public attention for treating retinal degenerative diseases such as retinitis pigmentosa (RP) and agre-related maculart degeneration (AMD). The device can deliver video data came from camera to retina through wireless transceiver [10].

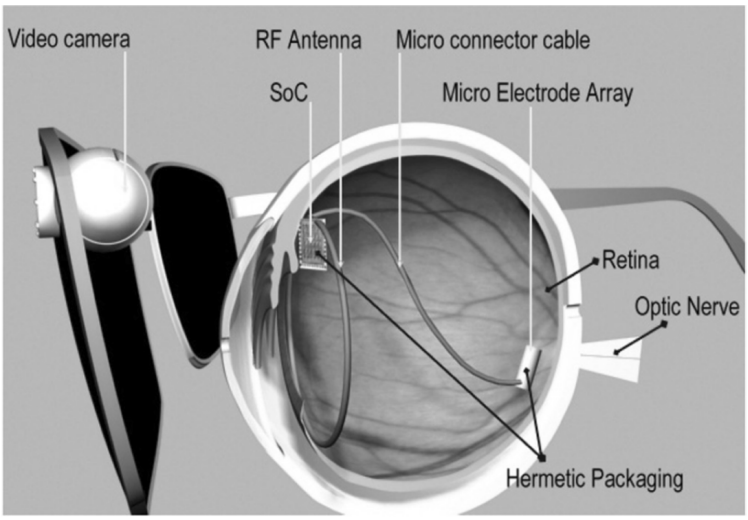

Fig. 1.3 System overview of an epiretinal prosthesis [10].

The advanced pace maker integrated with a transmitter can monitor a heart rate and remaining battery capacity [11]. The stent which is inserted to a blood vessel also can be integrated with a transmitter [12] for the monitoring for a blood pressure and flow.

In addition, the various medical sensors are suggested for the monitoring of the vital signs. The gathered data is transmitted to off-body receiver or wearable devices. The real and long-time monitored data can be used for the diagnosis. Also, the emergency such as a heart attack or stroke can be estimated through the change of vital sign can alter the hospital directly. The WBAN is a promising technology for the future medical services

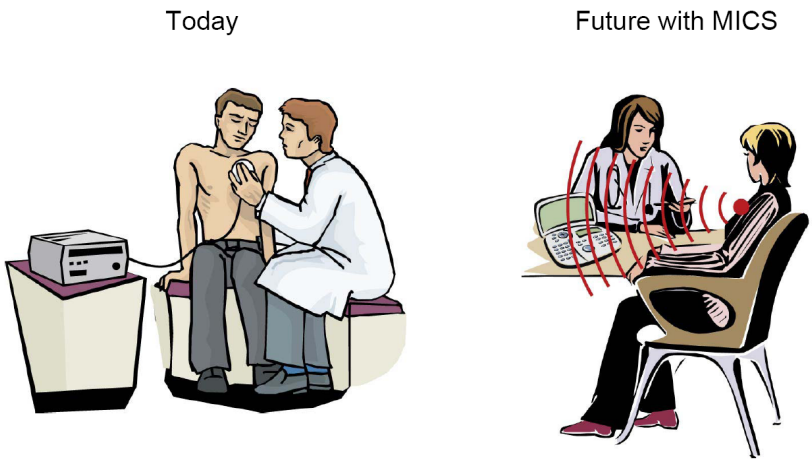

(a) Doctor's Office

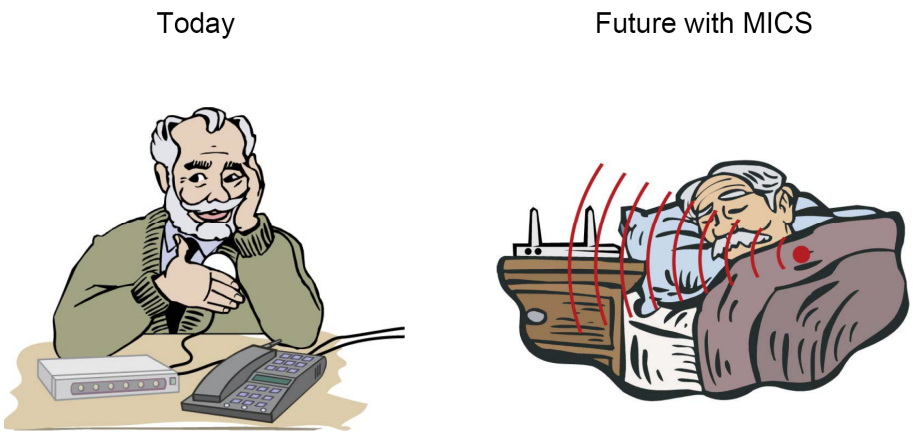

(b) Home monitoring

Fig. 1.4 Change of future medical services with WBAN

Several frequency bandwidths are allocated for the WBAN servicers. The MICS (Medical Implant Communication Service) is allocated from 402 MHz to 205 MHz for the implant services. The FCC has approved the allocation 40 MHz, from 2.36 to 2.3 GHz, for the medical low-power BAN links. WBAN services also can utilize the Wi-Fi bands for the data transmission.

The most important issue in designing WBAN system is an efficiency problem. As the transmitting power of the embedded and wearable devices are limited by SAR (Specific Absorption Rate) regulations and battery capacity, the system efficiency is especially important in WBAN systems. And, the electric properties of the human body make a high propagation loss between in and out body. Low power and efficient transceiver is essential in designing the high efficient WBAN system.

1.2 Challenges in Designing Transceiver for Implantable Medical Application

The first issue of implantable medical applications is finding an optimum frequency bands for alleviating a propagation loss and reducing the burden of device. The frequencies allocated by FCC are not suitable for implantable medical application due to its high lossy bands. And, the frequency bands allocated by MICS

are too narrow to cover high-data rate application such as capsule endoscopy, multi-channel electroencephalogram sensor, and epirentinal prosthesis. Therefore, we need find the optimum frequency bands for implantable medical devices by using analytical method.

The second issue of implantable medical applications is low power consumption of device. The implantable medical device based on wireless with a restricted battery life. And, the high propagation loss in human body which has high relative permittivity and conductive makes the implantable device be required for high sensitivity. Therefore, we need to minimize the power consumption of devices for extend a life of battery and many function of device.

The third issue of implantable medical devices is energy usage or figure of merit for fair evaluation. There are many application of implantable medical device having different data-rate and output power depends on its practical application. Therefore, the reference factor needs proposed transmitter to be compared with the other devices fairly. In implantable medical transmitter, the energy usage is used for this reference factor presented as (1.1) equation. However, the energy usage does not consider output power of transmitter directly affects its total DC power consumption. In this thesis, the figure of merit is used for transmitter's evaluation instead of energy usage such as (1.2) equation [13].

$$Energy\ usage\ [J/bit] = \frac{DC\ power\ consumption\ [J/s]}{Data\quad rate\ [bit/s]} \tag{1.1}$$

$$FOM\ [J/bit/W] = \frac{Energy\ usage[J/bit]}{Output\ power[W]} \tag{1.2}$$

Chapter 2

Propagation Loss in Human Body

2.1 Introduction

The high propagation loss occurs when RF signal through into the human-body from inner body due to high conductivity of tissues. And, it makes the hard requirement of transceiver for wireless communication between in-body and out-body. Therefore, finding an optimum frequency band is important to alleviate a propagation loss and to reduce the burden of device.

In this thesis, the dielectric properties of a human body from Federal Communication Commission (FCC) are used for human model. As the electric properties of human-body depend on part of body as well as frequency, the properties of muscle across 0.01 to 6 GHz are used for human-body model in this

work. The information related the human-body model can be obtained from FCC [14] as shown in TABLE 2.1.

Table 2.1 Human-body model in FCC [14]

Freq.	**Avg. Brain**		**Avg. Skull**		**Avg. Muscle**	
[GHz]	**ε**	**σ**	**ε**	**σ**	**ε**	**σ**
0.01	247.6785	0.2251	53.7738	0.0828	159.9523	0.6445
0.1	68.4678	0.4417	21.4555	0.1184	66.1887	0.7306
0.2	56.0647	0.5078	19.1819	0.1350	60.8680	0.7644
0.3	51.8980	0.5528	18.3008	0.1491	58.9795	0.7913
0.4	49.7531	0.5910	17.7950	0.1630	57.9722	0.8172
0.5	48.4177	0.6265	17.4477	0.1772	57.3247	0.8438
0.6	47.4897	0.6610	17.1831	0.1921	56.8596	0.8720
0.7	46.7965	0.6955	16.9674	0.2078	56.4996	0.9022
0.8	46.2513	0.2243	16.7833	0.2243	56.2056	0.9345
0.9	45.8055	0.7665	16.6208	0.2416	55.9555	0.9692
1	45.4296	0.8036	16.4738	0.2598	55.7358	1.0062
1.1	45.1048	0.8420	16.3383	0.2787	55.5381	1.0456
1.2	44.8183	0.8819	16.2118	0.2985	55.3565	1.0875
1.3	44.5613	0.9232	16.0922	0.3190	55.1870	1.1318
1.4	44.3258	0.9660	15.9783	0.3401	55.0267	1.1785
1.5	44.1121	1.0104	15.8690	0.3621	54.8735	1.2276

1.6	43.9116	1.0563	15.7635	0.3847	54.7258	1.2792
1.7	43.7233	1.1039	15.6614	0.4079	54.5824	1.3331
1.8	43.5449	1.1531	15.5620	0.4317	54.4423	1.3894
1.9	43.3749	1.2039	15.4651	0.4561	54.3048	1.4480
2.0	43.2120	1.2562	15.3703	0.4811	54.1693	1.5089

2.2 Far field approximation in human-body

The propagation loss can be calculated using Friss's formula considering transmission loss of body. However, the formula only validate in case of far-filed condition. Therefore, we need calculates wave length in human-body. Using electromagnetic theory in lossy medium [15], the electrical wave-length at each frequency can be calculated through equations shown below:

$$\lambda = \frac{2 \cdot \pi}{\beta} \tag{2.1}$$

$$\beta = \mathrm{Im}\left[j \cdot 2 \cdot \pi \cdot f \cdot \sqrt{\mu_0 \cdot \varepsilon} \cdot \left(1 + \frac{\sigma}{j \cdot 2 \cdot \pi \cdot f \cdot \varepsilon} \right)^{0.5} \right] \tag{2.2}$$

The λ is electrical wave-length and β is wave constant in lossy medium. f is frequency and σ is conductivity. μ_0 is permeability in air and ε is permittivity. We can obtain wave-constant from equation (1.4). Finally, electrical wave-length can be calculated from equation (1.3). The calculated results using human-body model at each frequency are shown below:

Table 2.2 Calculated results of wave-length in human-body (muscle)

Freq. [GHz]	**Human-body model [S/m]**		**Calculated results [m]**
f	**Permittivity**	**Conductivity**	**Electrical wave-length**
0.01	159.9523	0.6445	1.166
0.1	66.1887	0.7306	0.29
0.2	60.8680	0.7644	0.172
0.3	58.9795	0.7913	0.122
0.4	57.9722	0.8172	0.094
0.5	57.3247	0.8438	0.077
0.6	56.8596	0.8720	0.065
0.7	56.4996	0.9022	0.056
0.8	56.2056	0.9345	0.049
0.9	55.9555	0.9692	0.044
1	55.7358	1.0062	0.04
1.1	55.5381	1.0456	0.036
1.2	55.3565	1.0875	0.033
1.3	55.1870	1.1318	0.031
1.4	55.0267	1.1785	0.029
1.5	54.8735	1.2276	0.027
1.6	54.7258	1.2792	0.025
1.7	54.5824	1.3331	0.024
1.8	54.4423	1.3894	0.022
1.9	54.3048	1.4480	0.021
2.0	54.1693	1.5089	0.02

From Table 2.2, the far field approximation is validated in human-body model across 10 MHz to 2 GHz. Therefore, the friss's formula can be used for calculating the propagation loss in human body.

2.3 Calculation of a propagation loss in human-body

2.3.1 Friss's formula

Given the information of Table 2.2, the propagation loss can be calculated through the Friis's formula [16], considering the transmission loss in a body, as shown in equation (2.3). The formula should be used only if R is larger than λ, which is proved in human body model at hundreds of MHz due to its high permittivity in section 2.2. The Fig. 2.1 is shown as conceptual figure in propagation loss calculation and the meanness of all parameters in equation (2.3).

$$\frac{P_{RX}}{P_{TX}} = G_T \cdot G_R \cdot T^2 \left(\frac{\lambda}{4 \cdot \pi} \right)^2 \cdot e^{-2 \cdot |\mathrm{Im}[k]| \cdot R} \tag{2.3}$$

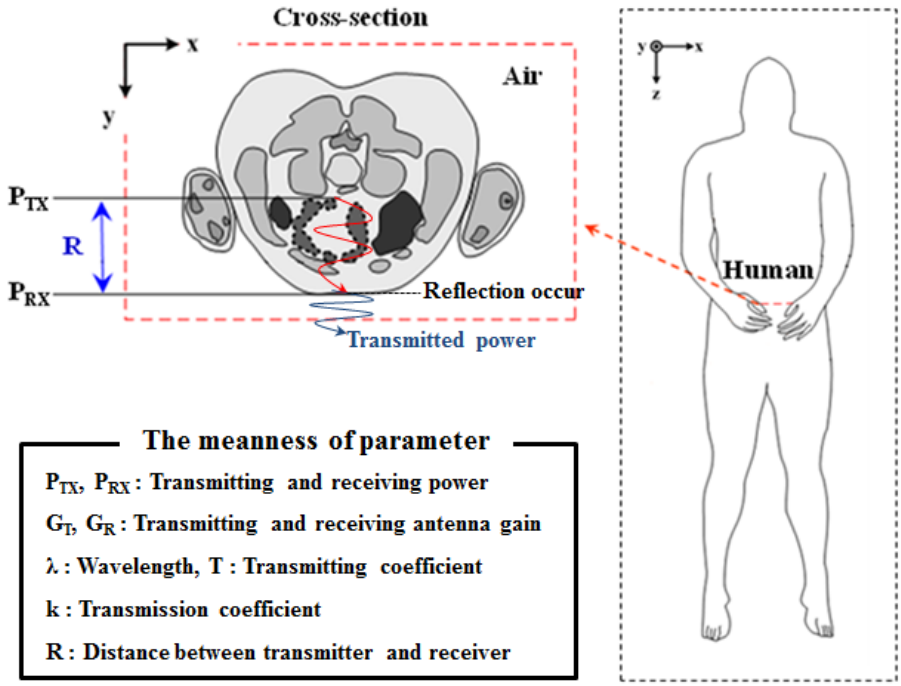

Fig. 2.1 Conceptual figure in propagation loss calculation

The equation shows the total loss that consists of the antenna gains, the radiation loss as well as the attenuation and reflection. In the analysis, G_R is assumed as unity gain since the physical dimensions of receiving antenna are not strictly limited at outside body. However, G_T should be obtained from equation (2.4) [17].

$$G_T = E \cdot D \tag{2.4}$$

Where, E is efficiency and D is the directivity of transmit antenna. In general,

the transmitting antenna for implantable device is smaller than the wavelength of operating frequency. Therefore, it is assumed that the directivity of the small antenna is defined 1.5 [18].

2.3.2 Efficiency of transmitting antenna in human-body

The efficiency of transmitting antenna could be obtained from the spherical modes analysis. The spherical modes are divided into two parts, which consist of Transverse Magnetic (TM) mode and Transverse Electric (TE) mode. The modes are related with dipole and loop antenna respectively.

If the antenna regards as small antenna, its efficiency is determined by each lowest order mode as the equation (3.17) in [19]. However, the antenna's bandwidth effect is not considered in that equation and it should be included in the analysis. The gain of antenna including its bandwidth is as in equation (2.5) [20]. Therefore, TM and TE mode antenna gain could be obtained. Moreover, T^2, λ, k can be obtained from electromagnetic theory in a lossy medium [15].

$$E = \begin{Bmatrix} \dfrac{Q_{required}}{Q} \cdot E_{eff}\Big|_{TM} & TM \text{ mode} \\ \dfrac{Q_{required}}{Q} \cdot E_{eff}\Big|_{TE} & TE \text{ mode} \end{Bmatrix} \tag{2.5}$$

$$Q_{required} = \frac{2 \cdot \omega_0}{Half - Power\ Bandwidth} \tag{2.6}$$

$$E_{eff} = \begin{Bmatrix} \dfrac{\mathrm{Re}(\eta)}{\mathrm{Re}\left\{ j \cdot \eta \cdot \hat{H}'_n(ka) \cdot \hat{H}_n(ka)^* \right\}} & TM \text{ mode} \\ \dfrac{\mathrm{Re}(\eta)}{\mathrm{Re}\left\{ -j \cdot \eta \cdot \hat{H}_n(ka) \cdot \hat{H}'_n(ka)^* \right\}} & TE \text{ mode} \end{Bmatrix} \tag{2.7}$$

$$Q = \begin{Bmatrix} \left(1 - E_{eff}\big|_{TM} \cdot e^{-2 \cdot |\mathrm{Im}[k]| \cdot a}\right) \cdot \cot(\delta) & TM \text{ mode} \\ E_{eff}\big|_{TE} \cdot \left(1 - \dfrac{1}{E_{eff}\big|_{TM}} \cdot e^{-2 \cdot |\mathrm{Im}[k]| \cdot a}\right) \cdot \csc(\delta) & TE \text{ mode} \end{Bmatrix} \tag{2.8}$$

$$\eta = \sqrt{\frac{z}{y}} \tag{2.9}$$

$$k = \sqrt{-y \cdot z} \tag{2.10}$$

$$z = j \cdot \omega \cdot \mu_0 \tag{2.11}$$

$$y = j \cdot \omega \cdot \varepsilon \cdot \varepsilon_0 + \sigma \tag{2.12}$$

$$\delta = \arctan\left(\frac{\sigma}{\omega \cdot \varepsilon \cdot \varepsilon_0} \right) \tag{2.13}$$

2.4 Calculation of propagation loss in human-body and conclusion

The total propagation losses are shown Fig. 2.2 on the condition of antenna's dimension, a, = 5 mm and minimum antenna's bandwidth = 100 MHz, R = 15 cm. The graph includes the losses of the transmitting antenna's gain, the radiation, the attenuation and the reflection. Its propagation loss is validated only if R is larger than λ.

In the results, the minimum total losses in the human body are shown to be approximately 59 dB at a frequency of 400 - 600 MHz when a loop antenna is used. And, the losses are 66 dB at same frequency bands when a dipole type is used. From

this result, we adopt operation frequency for implantable medical transmitter as 500 MHz to minimize the propagations loss in human-body.

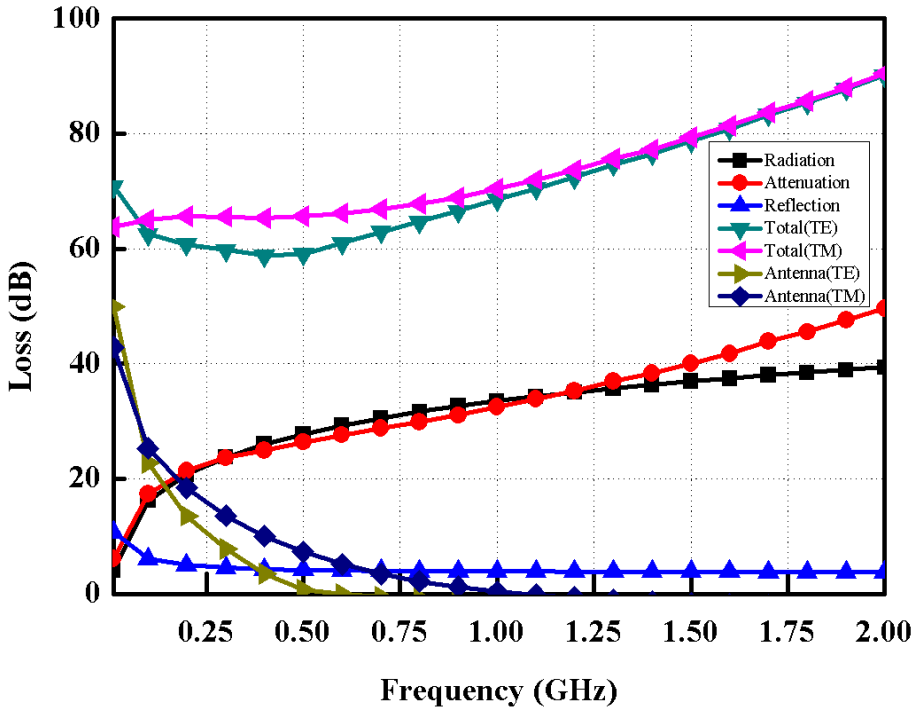

Fig. 2.2 Calculated propagation loss in human-body

Chapter 3

A Design of Transceiver for Capsule Endoscopy Application

3.1 Introduction

An endoscope is an essential device in medical applications for its ability to examine the digestive tract accurately. However, it is inconvenient to use in a conventional wired endoscopy system because wired endoscopy causes considerable discomfort to patients. Also, the conventional instrument is limited in terms of its test coverage due to its finite length. Moreover, in the long and twisted small intestine, it is cannot easily access all of the digestive organs. These issues are directly related to the quality of the diagnosis. Therefore, many novel endoscopy

examination methods, such as ultrasound detection and wireless telemetry, have been developed [21]-[22].

Among them, the wireless capsule system whom Iddan was the first to describe is suitable for a substitution device of conventional endoscopy [6]. It could be small enough to be swallowed by patients without causing any discomfort. And, the capsule system has the advantage of offering a means of direct examination of the entire digestive tract with no anesthesia or insufflations [23]-[24].

In a capsule endoscopy system, the system bandwidth is an important issue related to the accuracy of the diagnosis. As the digital communication data rate is proportional to the capsule system bandwidth [25], the bandwidth should be wide enough to handle the transmission of high-resolution image data in real time. In real environments, as the movement of the locomotive capsule is affected by the speed of peristalsis, high quality image data is advantageous for accurate diagnoses [26], [27].

The existing system has a data rate of about 1-2 Mbps [28], [29] and it is difficult to render a smooth real-time image, as its frame rate is generally about 5fps or less. In the biomedical industry, Zarlink and Toumaz technologies have developed the devices for biomedical sensor which also have low data rate [30], [31]. Recently, a high-speed system capable of 10 Mbps at 3-5 GHz was introduced [32]. However, this system did not an adequate frame rate and its capsule size was too large for

patients to shallow it. Another solution for a high frame rate was introduced as a compression technique, but this technique increases complexity of the modem and consumes a considerable amount of power [33]. Generally, the data rate is inversely proportional to the efficiency. Therefore, implementation of a high frame rate and a high-efficiency system is not straightforward.

This paper presents the high-speed and high-efficiency capsule endoscopy system by optimizing the system at 500 MHz. The issue about the optimum frequency bands for wireless telemetry in human body was already discussed about the aspect of electromagnetic filed in [17]. However these results can not directly suggest the link budget for a system design. Therefore, the link budget was calculated from the propagation loss of the human body channel in chapter 2. A transmitter and receiver were implemented in the 0.13 μm CMOS process and each system performance was verified in section 3.3. Simultaneously, Considering the space limitation for transmitting antenna at 500 MHz, the system adopts an outer wall loop antenna that reduces the capsule size and offers better performance than a helical antenna or a planar spiral antenna [18], [34], [35]. Finally, through an image recovery experiment in a liquid human phantom and in the digestive organs of a live pig, the designed system was tested in section 3.4.

3.2 System link budget calculation

Although the loop types are more efficient than the dipole types in the conductive material such as the human body, the loop types have realization issue [19]. Therefore, the TM total loss in Fig. 2.2 in chapter 2 was chosen for link-budget calculation.

From the previously calculated propagation loss analysis, the optimum frequency to minimize the propagation loss is determined to be 500 MHz. The system bandwidth is set to 20 MHz to support a data rate of 20 Mbps. The output power of the transmitter was set to -3 dBm, which is the average power. The receiving antenna gain is set to -10 dB with a 3 dB margin. Table 3.1 shows the link budget configuration. The sum of the total loss in the body is -72 dB. Therefore, the expected receiving power is -72dB considering the transmitting power. On the other hand, the thermal noise power is calculated as -101 dBm at 300 K when the data rate is 20 Mbps. From the noise power, if the envelope detector has a Signal-to-Noise Ratio (SNR) of 14 dB at 10^{-5} BER theoretically, the receiver's SNR is -82 dB including the receiver's noise figure (5 dB). This result has an expected receiving power margin of 10dB. The margin is important in the analysis, as the homogeneous human body model is not quite valid and because personal variations exist. This can

make antenna matching or propagation loss problems.

Table 3.1 Link budget of OOK system for a wireless capsule endoscope

<table>
<tr><td>Frequency band 490 MHz – 510MHz
(OOK, 20Mbps)</td><td colspan="2">Power</td></tr>
<tr><td>Power of transmitter</td><td>- 3 dBm</td><td rowspan="3">- 72 dBm</td></tr>
<tr><td>Antenna gain</td><td>- 7 - 3 dB</td></tr>
<tr><td>Propagation + Radiation
+ Reflection</td><td>- 59 dBm</td></tr>
<tr><td>Link margin</td><td colspan="2">10 dB</td></tr>
<tr><td>Noise figure of receiver</td><td>5 dB</td><td>- 82 dBm</td></tr>
<tr><td>SNR (Env. Detection, BER 10^{-5})</td><td>14 dB</td><td>- 87 dBm</td></tr>
<tr><td>Thermal noise power</td><td>- 101 dBm</td><td>- 101 dBm</td></tr>
</table>

3.3 Implementation

3.3.1 Transmitter with class B amplifier

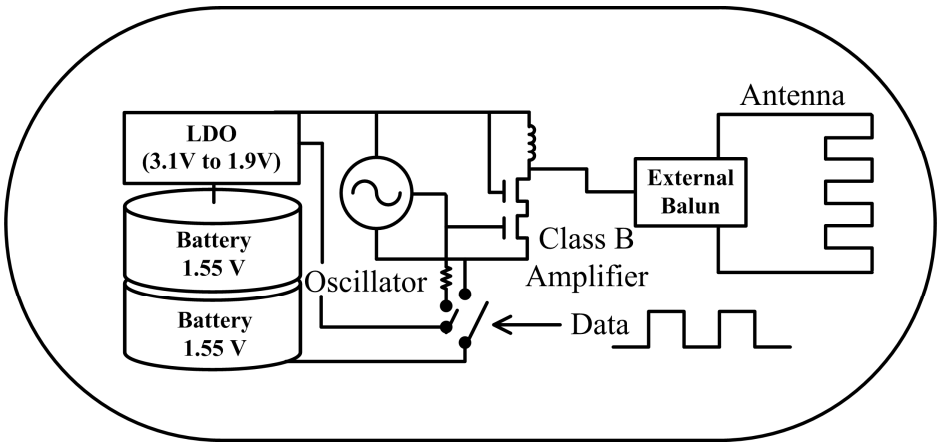

Fig. 3.1 OOK transmitter for a capsule endoscopy

A simple structure should be implemented in the capsule system for high-speed and low power. Therefore, OOK modulation is utilized. The structure of the transmitter is shown in Fig. 3.1. For a high efficiency, all components should be switched On/Off by baseband data with a falling and rising time less than 10 ns to guarantee a 20Mbps data rate [36].

The transmitter uses Renata 394 (1.55 [V]) type batteries (two in series), which may cause to critical problems such as variations in the output power and the center frequency in the transmitter during operation. Therefore, the LDO regulator, a DC linear voltage regulator, is adopted to stabilize the supply at 1.9[V] independent of the battery voltage.

A ring oscillator has faster start-up time than an LC oscillator [37]. And, the operation frequency can be controlled without an external passive inductor. Moreover, a ring type has good stability in the human body maintaining a constant temperature. Therefore, a ring type oscillator was adopted for high-speed system.

For achieving a good efficiency and output power, a class B amplifier was chosen for our system. The class B amplifier has an On/Off characteristic depending on input data. Also, the gate bias 500 mV is switched by input data, which could save a leakage power.

3.3.2 Super-heterodyne receiver with AGC

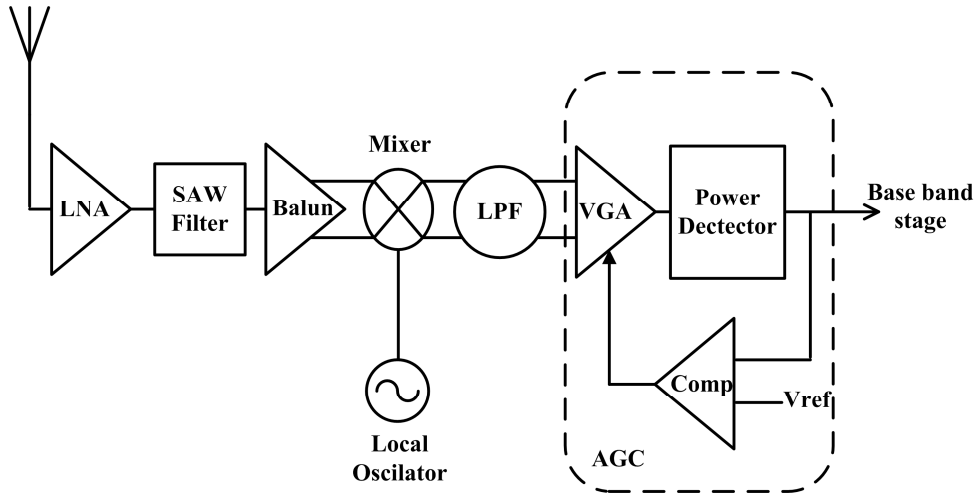

Fig. 3.2 Super-heterodyne receiver with AGC for a capsule endoscopy

The receiver could compensate the large attenuation signal through the human body by using a super-heterodyne architecture, as shown in Fig. 3.2. The structure could divide a receiver's gain into Radio Frequency (RF) and Intermediate Frequency (IF) gains, which reduce the unwanted interaction between the RF and IF stages. Therefore, it can produce a good stability of the receiver despite its high gain.

Using a proposed structure, the RF and local frequency are set to 500 MHz and

400 MHz, respectively. An Automatic Gain Controller (AGC) was utilized at the IF stage to cover changes in the received signal power according to the location of the capsule endoscopy [38]. Also, the differential signal processing was used for reducing unwanted common mode noise bounds. It was established by adopting a active balun for integration. Every circuits are implemented as conventional structure such like cascode Low Noise Amplifier (LNA), Gilbert-type mixer, Chebyshev-type active Low Pass Filter. However, an Surface Acoustic Wave (SAW) filter (SA500AP) provided from SAWNICS (http://www.sawnics.com) was externally used to remove out-of-band interference signals. Its steep skirt performance could reject unwanted signal and a SAW is generally used in mobile communication.

3.3.3 Measurement results

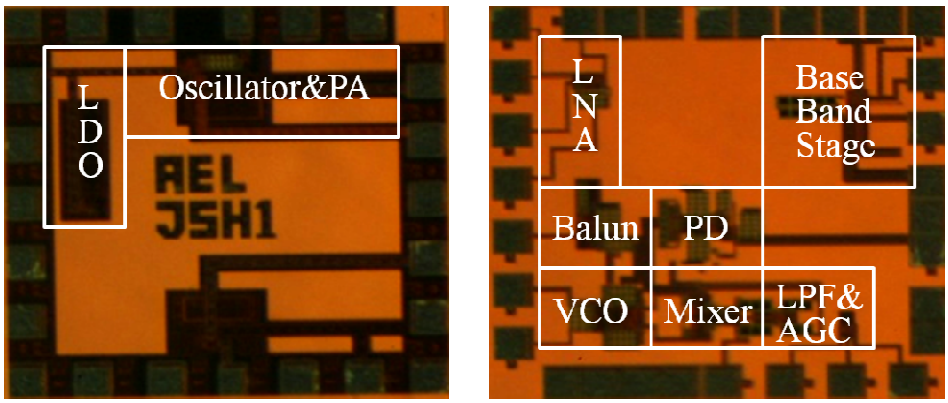

Fig. 3.3 Microphotograph of designed system: transmitter and receiver.

The transmitter and receiver were fabricated using 0.13 m CMOS process with each die area of 1 mm x 1 mm as shown in Fig. 3.3. The Fig. 3.4 (a) shows the output spectrum in the frequency domain when a data from CMOS camera is delivered to designed transmitter. The result shows the center frequency and its peak power shown 500 MHz and -3.72 dBm respectively. When the transmitter is in an on/off state, the modulation makes the power spread in a certain frequency range. Therefore, the channel power is measured with the 20MHz channel bandwidth, as shown in Fig. 3.4 (b).

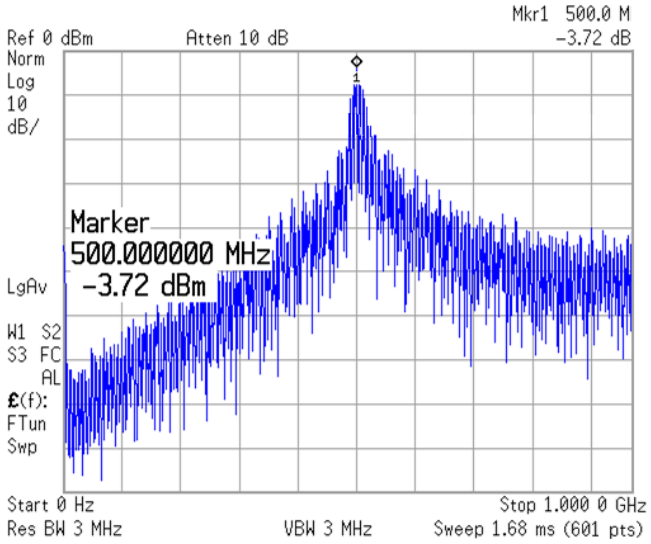

(a)

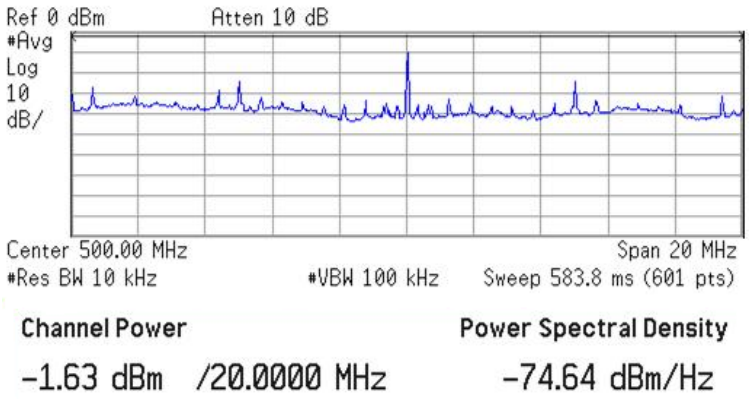

(b)

Fig. 3.4 The transmitter measurement results : (a) output spectrum (b) average channel power in 20 MHz

From the measurements, the overall efficiency of the transmitter including the LDO is 27.7 % with an output power of -1.6 dBm at a 3.1 [V] supply. However, the efficiency, a ratio of the output power to the total dissipated power, is 41 % at a 2.1 [V] supply when the battery is discharged. Finally, Table 3.2 shows features of the transmitter capsule. Its performance satisfies the requirements of the link budget in section 3.2.

Table 3.2 Feature of designed transmitter for a wireless capsule endoscope

Data rate	20 Mbps
Average power / Output power of transmitter	0.7 mW / -1.6 dBm
Efficiency of transmitter at 3.1 [V] battery	27.7 %
Technology (CMOS)	0.13 μm
Carrier frequency	500 MHz
Chip Area	1 mm^2

Since every circuits are integrated in single chip at the designed receiver, only a BER test and LNA measurements are performed. The LNA with SAW filter was measured with Vector Network Analyzer as shown in Fig. 3.5. It presents a good skirt performance and a gain of 18 dB including the SAW filter's insertion loss.

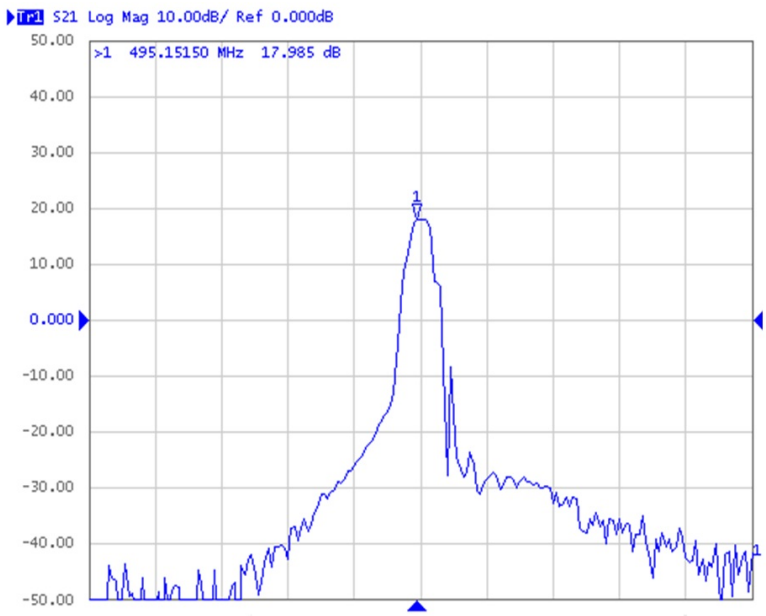

Fig. 3.5 Small signal gain of LNA with SAW filter at vector network analyzer

Table 3.3 Feature of designed receiver of a wireless capsule endoscope

Data rate/BER	20 Mbps / $< 10^{-5}$
Average DC power	22.8 mW
Sensitivity	- 80 dBm
RF / IF	500 / 100 MHz
Input dynamic range	-50 to -80 dBm
Supply voltage	1.2 [V]
Technology	0.13 μm
Chip Area	1 mm^2

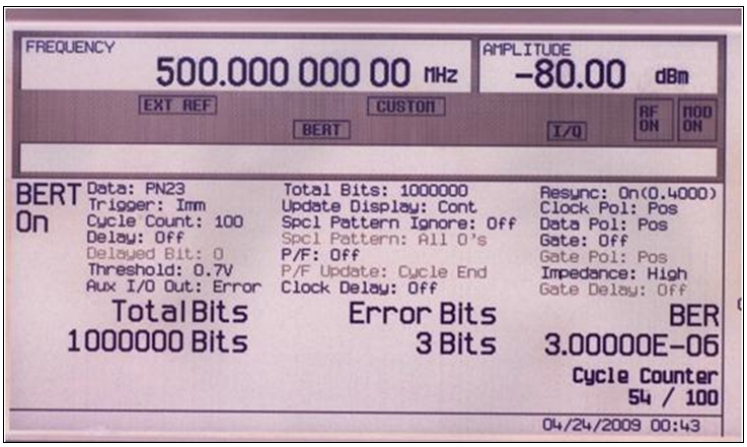

Fig 3.6 Bit-Error-Rate test results at Agilent E4438C

To measure the sensitivity of designed receiver, a BER test was performed with a PN23 random OOK signal. The receiver showed sensitivity of -80 dBm with a BER value of 3 x 10-6 at a data rate of 20 Mbps. The dissipated DC power of the receiver is 22.8 mW at this test condition. Fig. 3.6 shows the results of the BER test using the E4438C signal generator (Agilent). The sensitivity of the receiver satisfies the link budget calculated in previous section. Table 3.3 shows the features of the designed receiver for a capsule endoscopy system.

3.4 Image recovery experiment

3.4.1 Integration of capsule endoscopy

The integrated capsule consists of several parts. It includes a CMOS camera and a transmitter, the antenna, and the batteries. Fig. 3.7 shows the integrated capsule transmitter and the components. All of the components are covered with a plastic capsule shell with a diameter of 12.5 mm and a length of 30 mm. The CMOS camera is provided by a company from I3SYSTEM (http://www.i3system.com). An

outer wall loop antenna that is dipole type is adopted to reduce the capsule size and to ensure a high gain. A conventional balun (B0322J5050A00) provided from Anaren (http://www.anaren.com/) is used for the connection between the antenna and the transmitter as shown Fig. 3.1, because the differential type of antenna used here. To connect the balun to the antenna, two holes were made with a drill on the shell, and both devices were soldered with two thin metal wires through each hole as shown Fig. 3.8.

Fig. 3.7 Photo of the integrated capsule endoscopy

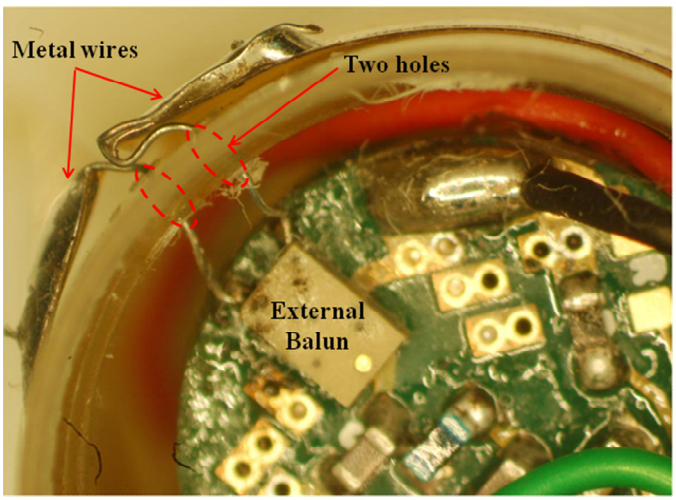

Fig. 3.8 Connection between balun and antenna

3.4.2 Image recovery in the liquid human phantom

A liquid human phantom presents an environment similar to that of a human or a pig. It is a mixture of several materials, and its electrical properties are same as the average values of characteristics of human organs such as the conductivity or permittivity. Therefore, an experiment using a liquid human phantom presents a good reference for an the animal test.

To verify the system operation, image tests were performed in the liquid human phantom [39]. Fig. 3.9 (a) shows the measurement setup applied during the image recover test. The receiving antenna adopted a buffer layered type for low reflection loss [40]. I3SYSTEM company provides the modem and the PC software to decode the transmitted data. Fig. 3.9 (b) show the actual object (left) and image captured (right) respectively. The recovered image suggests that an each system described in section 3.4 could operate well together in the environment which is similar to the human body.

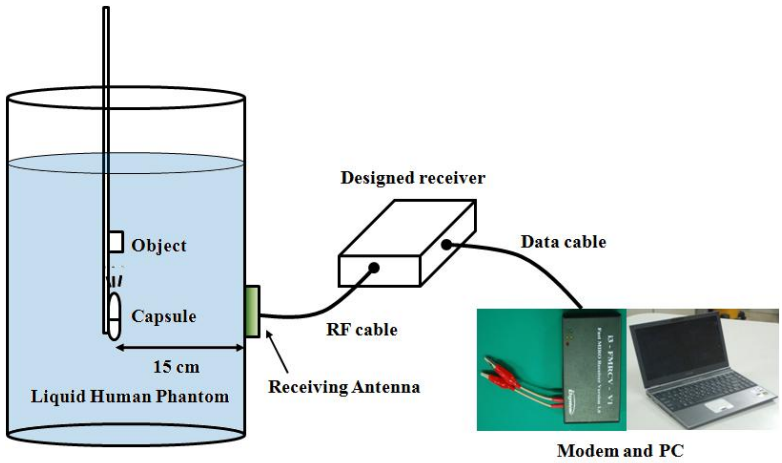

(a)

(b)

Fig. 3.9 Image recovery test in the liquid human phantom: (a) Measurement setup (b) Actual object (left) and captured image (right)

3.4.3 Image recovery in a pig's stomach and large intestine

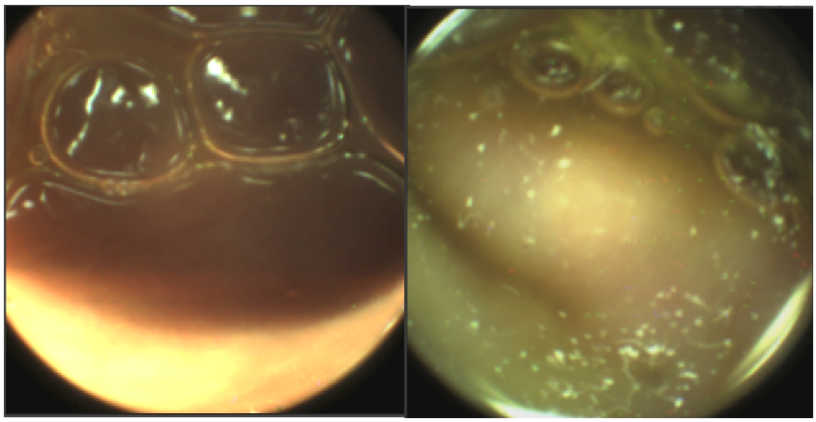

Fig. 3.10 Image recovery test in the aliving pig : (a) stomach wall and (b) large intestine wall

The image recovery was also performed by using alive pig to verify the system operation in more practical case. The measurement setup is almost same in [25]. The capsule camera transmits images having a 340 x 340 pixel resolution at 10.5 f/s without using a compression technique. Fig. 3.10 shows the resulting images in the pig's stomach and large intestine. In the pig's stomach and large intestine, the high frame images were recovered through the designed system. This result can ensure

the validation of our system for wireless capsule endoscopy with high data rate and low power consumption.

3.5 Conclusion

An optimized system for a capsule endoscope is presented through the link budget calculation in this thesis. The system is implemented in a 0.13 μm CMOS process and verified through measurement. Also, an outer loop antenna was used for the small capsule design. The designed system has been successfully operated in liquid human phantom and in a live pig. Therefore, the designed low power system is well suited for high-speed capsule endoscope system.

Chapter 4

Super-Regenerative Receiver with Digitally Self-Quenching Loop

4.1 Introduction

In WBANs, some application such as capsule endoscopy, epiretinal prosthesis, multi-channel electroencephalogram sensor needs a receiver having low-power and high-data rate. A high data rate is required to transmit high-resolution images for accurate diagnoses when using a capsule endoscope. Also, in case of receiver at out-body or on-body, these issues are important to utilize the home healthcare not going to hospital. The receiver should be integrated with mobile device and be played a

role as personal health server in the future. We could be diagnosed by doctor not going hospital through internet and check our life states using mobile and implantable devices. Therefore, develop of low power and high-speed receiver is essential for the home healthcare.

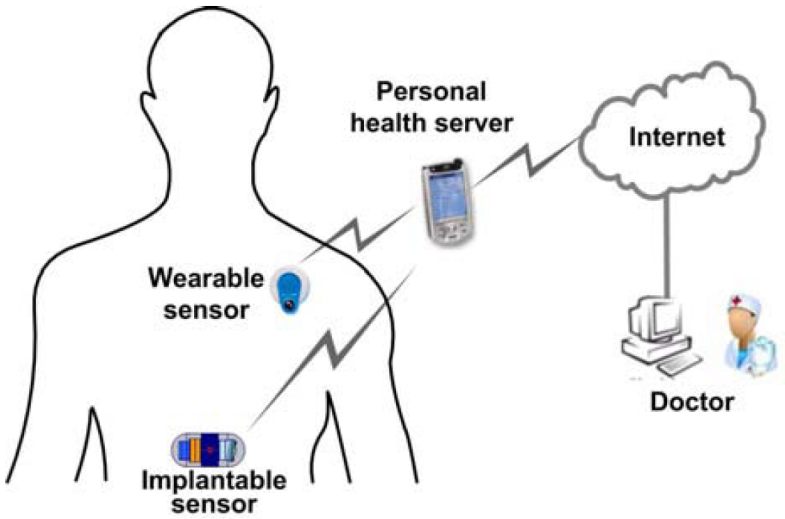

Fig. 4.1 Wireless telemetry system for healthcare application [32]

4.1.1 Selection of receiver's architecture for implantable medical device

Wireless communications have been developed for more than a century. There are several classical receiver architectures such as super-heterodyne, direct-conversion and super-regeneration. Usually different receiver architectures match different applications depending on the system complexity, power consumption, external component count and system cost.

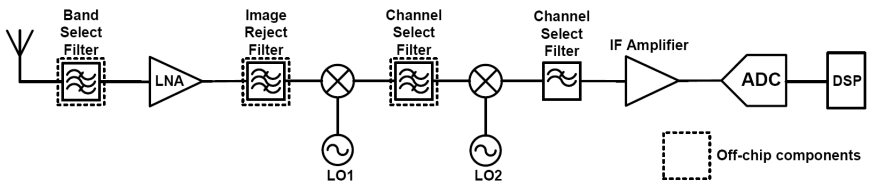

Fig. 4.2 Block diagram of super-heterodyne receiver

The super-heterodyne architecture is one of the most popular architecture in modern radio products. A super-heterodyne receiver converts the received RF signal

to an intermediate frequency (IF). Therefore good frequency isolation between RF signal and local oscillator (LO) is achieved, and the radiation from the local oscillator is minimized. Furthermore, amplification is distributed across several frequency stages which relaxes the gain and stability requirement in each stage and increases the total possible gain. Generally a super-heterodyne receiver provides good frequency selectivity and high sensitivity. But it has several drawbacks. In this architecture several filters are required for band selection, image rejection and channel selection. And the filters are usually bulky, expensive SAW filters, which can't be integrated on chip, and greatly increase the physical size and cost of the system.

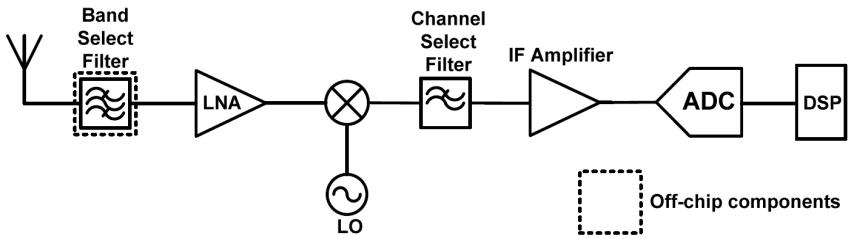

Fig. 4.3 Block diagram of a direct-conversion receiver

The direct-conversion architecture is another popular architecture in modern wireless receivers. Due to its high level of integration, this architecture has been found in more applications recently, especially in multi-standards wireless communications. In a direct-conversion receiver, the received RF signal is converted to DC or low IF. The image signal is at the desired signal frequency, so no image rejection filters are required. Thus direct-conversion receiver is suited to on-chip integration. But there are several drawbacks, which make it inferior to super-heterodyne receivers in the past. DC offset is probably the most serious problem. Since, the down-converted band extends to zero frequency in a direct-conversion architecture, DC offset voltages break the signal and saturate the following stages. The DC offset is caused by LO leakage and interferer induced self-mixing. On the other hand, the flicker noise of CMOS devices also substantially corrupts the down converted zero frequency signal. There are other disadvantages such as I/Q mismatch in quadrature mixing and even order distortion. To overcome these problems, periodic calibration and offset cancellation techniques need. However, these increase circuit complexity and system power dissipation.

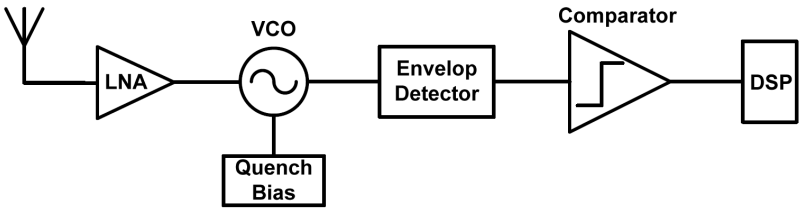

Fig. 4.4 Block diagram of a super-regenerative receiver

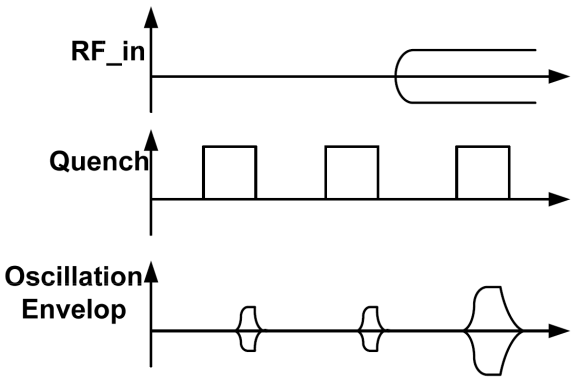

Fig. 4.5 Concept of a super-regenerative receiver

The super-regenerative architecture is based on the super-regeneration principle invented by Armstrong in 1922 [41]. This technology was usually used in vacuum tube circuits, but recently there has been a renewal of interest in this architecture.

The principle of super-regeneration is based on the variation of the start-up time of the oscillator. Normally oscillation starts from thermal noise in the circuit, which is a relatively slow process. When there is an injected external RF signal, such as a carrier at the resonance frequency, the startup becomes much faster. The oscillator is enabled by a quench signal, so it is periodically driven into the critical oscillating condition, or oscillation start-up state. OOK (On/Off Keying) modulation, or 100% amplitude modulation, is easily detected with this architecture.

Each architecture has its merits and drawbacks. Table 3.1 summarizes the pros, cons and applications for each architecture. The super-regenerative receiver provides large signal gain using only an oscillator as an amplifier with positive feedback, and no separate VCO is needed, which leads to lower power consumption. For this reason, super-regenerative architecture is chosen for implantable medical application.

Table 4.1 Comparison of different receiver architectures

Architecture	Pros	Cons	Applications
Super-heterodyne	High performance reliable	Good integration Large physical size High power High cost	Cellular Communication, Radar, GPS, WLAN
Direct-conversion	Good integration than super-heterodyn Low power Low cost	DC offset Flick noise Even order distortion I/Q mismatch	Multi-band cellular Communication radar, GPS, WLAN
Super-regenerative	Simple Small physical size Low power High level of integration	Poor selectivity and sensitivity	Short-range, low data rate

4.1.2 Previous study of super-regenerative receiver

A Super-Regenerative Receiver (SRR) is a suitable receiver structure for short-range wireless communications such as a Medical Implant Communication Service (MICS) and, a Wireless Sensor Network (WSN) due to its low power consumption and high gain. Therefore, various types of super-regenerative receivers have been developed for these applications [42]-[48].

To reduce power consumption in a SRR, [44], earlier work [47] used an initial calibration process to set the minimum receiver bias current for the optimum operation. These calibration processes are executed by digital circuits which consume its power only during the initial set-up time of receiver. Other research [46], [48] used quasi-static devices for data acquisition. Quasi-static devices consume power only when they receive an input signal.

4.2 Main idea of proposed super-regenerative receiver

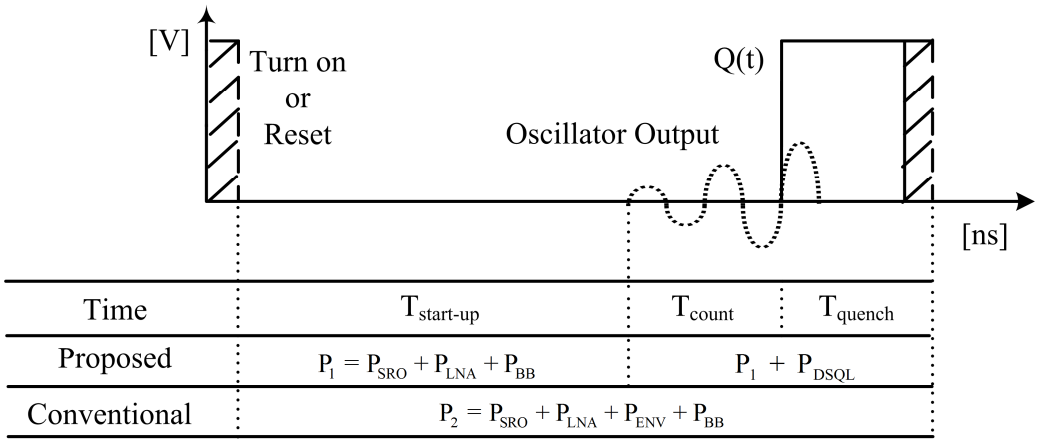

Fig. 4.6 Average power consumption of the proposed receiver and a conventional SRR receiver

Fig. 4.6 shows the conceptual power consumptions of two receivers, i.e., the conventional and proposed types, in the time domain. Generally, an envelope detector in a conventional SRR always consumes power. However, the DSQL in the proposed receiver does not consume any power during the start-up time of the SRO due to its zero idle current, which decreases the average power consumption of proposed receiver. Here, P_{SRO}, P_{LNA}, P_{DSQL}, P_{ENV}, and P_{BB} refer to the power consumed power at the SRO, LNA, DSQL, envelop detector, and base-band devices, respectively, including the filter, comparator and inverter. Therefore, the difference

in the power consumption rates between conventional structure and the proposed structure can be estimated by equation 4.1.

$$P_{rate} = \frac{P_1 \cdot T_{start-up} + P_2 \cdot (T_{count} + T_{quench})}{P_2 \cdot (T_{start-up} + T_{count} + T_{quench})} \tag{4.1}$$

$$\approx \frac{P_1}{P_2} = \frac{1}{1 + \dfrac{P_{ENV}}{P_{SRO} + P_{LNA} + P_{BB}}} \tag{4.2}$$

Here, $T_{start\text{-}up}$, T_{count}, and T_{quench}, refer to the start-up time, counting or enveloping time, and the quenching time respectively. If $T_{start\text{-}up}$ is much longer than the other times (T_{count}, T_{quench}), P_{rate} is identical to equation 4.2. Therefore, the proposed receiver with a DSQL can save power during the start-up time when the RF signal is not injected into SRO. This technique is efficient for high-speed application [48], [49] whose P_{ENV} is larger than that of low-speed application..

In this work, we analyze the SRR proposed in [50] in detail and show the measurement results of the fabricated chip, which operates under a reduced idle current through use of a Digitally Self-Quenching Loop (DSQL) with a two-bit digital counter. The DSQL with a zero idle current replaces the envelop detector in the conventional SRR structure and reduces the oscillation time of quench oscillator drastically. Therefore, the power consumption of the receiver is minimized and its

efficiency (nJ/bit) is maximized. The operating frequency of the SRR is set to 500MHz for in-body communication. The fabricated receiver with a 1 V power supply shows the minimum energy usage of 0.09 nJ/bit at 10 Mbps. Its measured sensitivity is -76 dBm with a Bit Error Rate (BER) of 10^{-3}.

4.3 Description of proposed receiver

Fig. 4.7 shows a block diagram of the proposed receiver, consisting of Low-Noise Amplifier (LNA), DSQL, a Super Regenerative Oscillator (SRO), and an active RC-filter with two inverters as the output buffer. The counter in the DSQL counts the number of crests of the SRO output and generates a quench pulse when the counter is full. The reset signal R(t) is a short time-delayed pulse of Q(t), which resets the counter immediately after a quench signal is issued. This process is repeated and the DSQL generates a periodic quench signal Q(t). Therefore, the SRO periodically starts up and shuts off according to the DSQL and the period of the quench signal is dependent on the start-up time of the SRO. When the RF signal I(t) is injected into the SRO by the LNA, the Q(t) period is decreased. Fig. 4.8 shows a operation of proposed receiver at time-domain. The data is recovered by monitoring the DC level at the output of the active RC-filter.

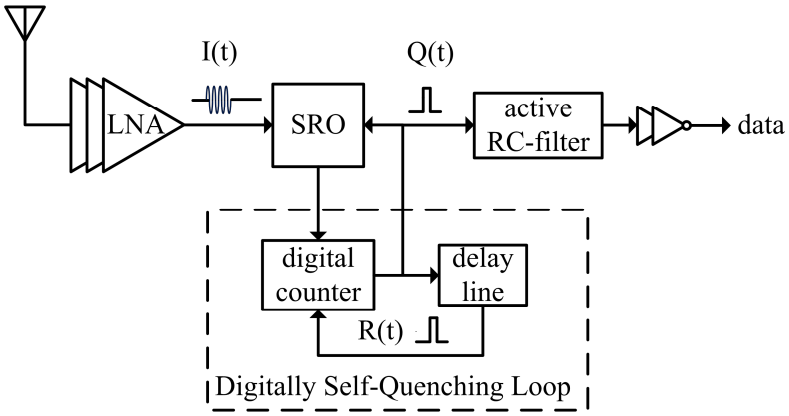

Fig. 4.7 Block diagram of proposed receiver

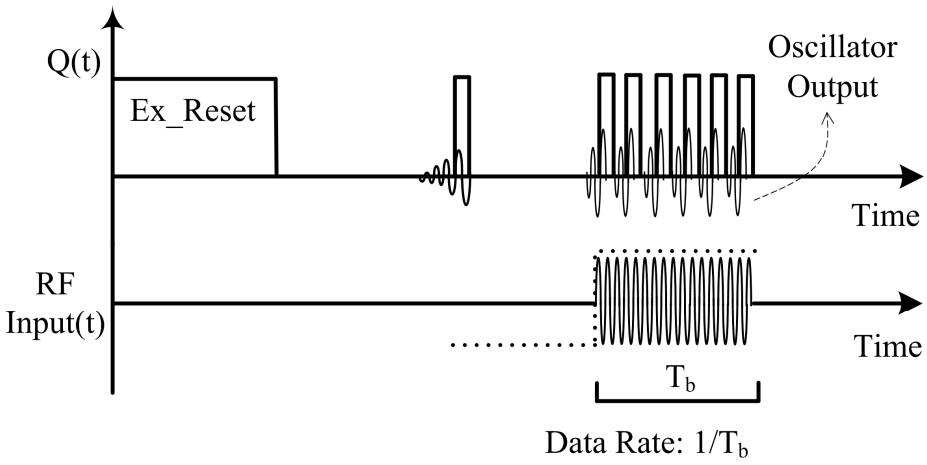

Fig. 4.8 Operation of proposed receiver at time-domain

4.3.1 Digital self-quenching loop

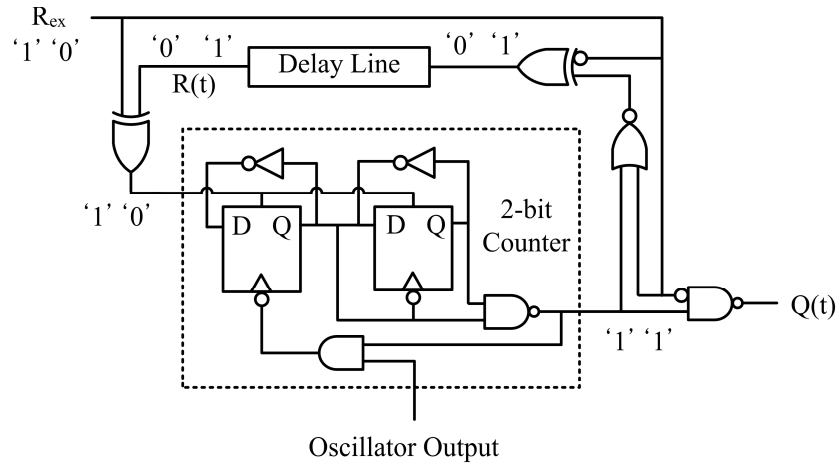

Fig. 4.9 Gate level schematic of the digital self-quenching loop

Fig. 4.9 shows the gate-level schematic of the DSQL, a simplified version, having a zero idle current during the start-up time of the SRO. A simple two-bit counter is used in the DSQL to minimize its power consumption and to increase the data rate so that it is proportional to the quench rate [49].

The external reset port R_{ex} shown in the figure is adopted to reset the DSQL initially. When the external reset R_{ex} is ‘1’, the quench signal Q(t) expresses ‘1’ to shut off the SRO. R_{ex} is then ‘0’, and all logic gates are operated as buffers and the

quench signal Q(t) is fixed at ‘0’. Next, the SRO starts up and runs, until the binary count number in two-bit counter is ‘11’. When the binary number changes to ‘11’, Q(t) transfers to ‘1’. This inactivates the SRO again. After a time delay, the DSQL is reset by R(t). R(t) is generated by Q(t) through the delay line, which consists of an inverter array. These operations repeat periodically until the DSQL is initialized by an external reset. The time duration of delay line in Fig. 4.9 is designed as 5 ns considering a data rate of 10 Mbps and Process Voltage Temperature (PVT) variations. The total quenching times related to the data rate are the sum of the reset time, oscillator start-up time, and counting time. To decrease the counting time, a 2-bit counter was used, which reduces the power consumption of oscillator

4.3.2 Low noise amplifier and super-regenerative oscillator

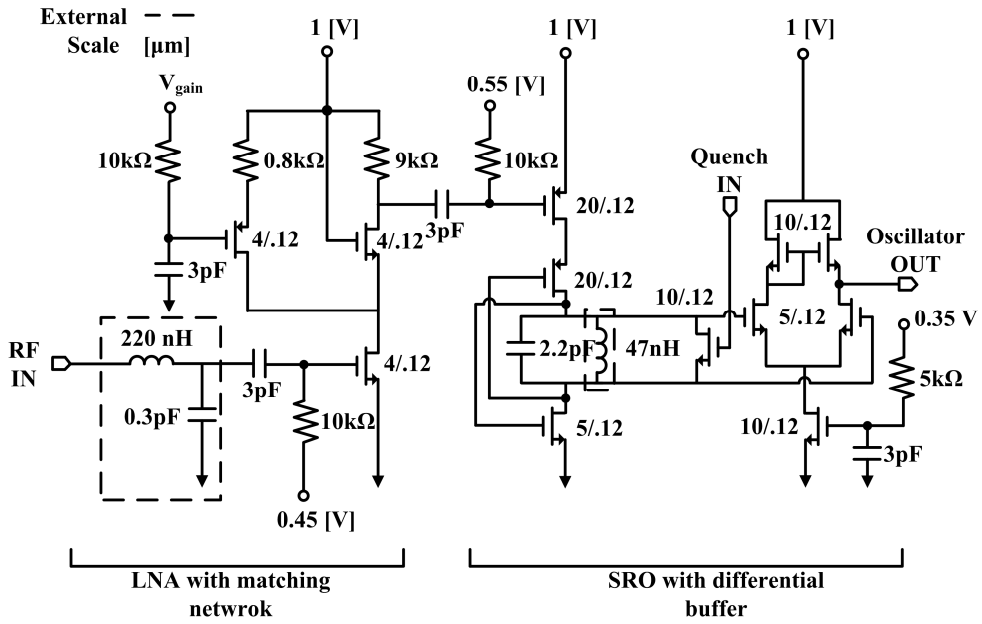

Fig. 4.10 Schematic of a LNA with a matching network and a SRO with a differential buffer

Fig. 4.10 shows the schematics of the LNA, and the SRO. The LNA is designed as a three-stage cascade structure to achieve high reverse isolation and gain, although only a single stage is presented in Fig. 4.10. All stages are identical to the amplifier shown in Fig. 4.10. In front of the first stage, a matching circuit externally

exists to match the antenna impedance.

The current bleeding technique is adopted to increase the gain by properly biasing V_{gain}. The high gain of LNA is essential for a good sensitivity of proposed receiver. A p-type transistor was used to prevent signal leakage into the bleeding circuit, since the impedance toward PMOS's drain was high enough. The resistor 0.8 kΩ is adopted to decrease the sensitivity of the bleeding circuit by bias voltage. This resistor is operated as a negative feed-back resister in the bleeding circuit.

The SRO is a current reuse type which is suitable for low-power and high-speed applications [51]. The RF signal is injected into the current source of the oscillator and it changes the start-up time. The 47 nH and 2.2 pF consist of LC-tanks for the oscillation frequency that should equal the injected signal frequency for high sensitivity. The switch is used for quenching the oscillator by controlling the quality factor of the LC-tanks. A differential buffer was adopted to deliver the signal to the controller. Generally, the differential buffer has a robustness of supply or else ground noise occurs from the bonding wires. It is good for the stable quenching operation. The SRO is biased near the sub-threshold voltage to maximize the start-up time and minimize its power consumption.

4.3.3 Active RC filter for low power consumption

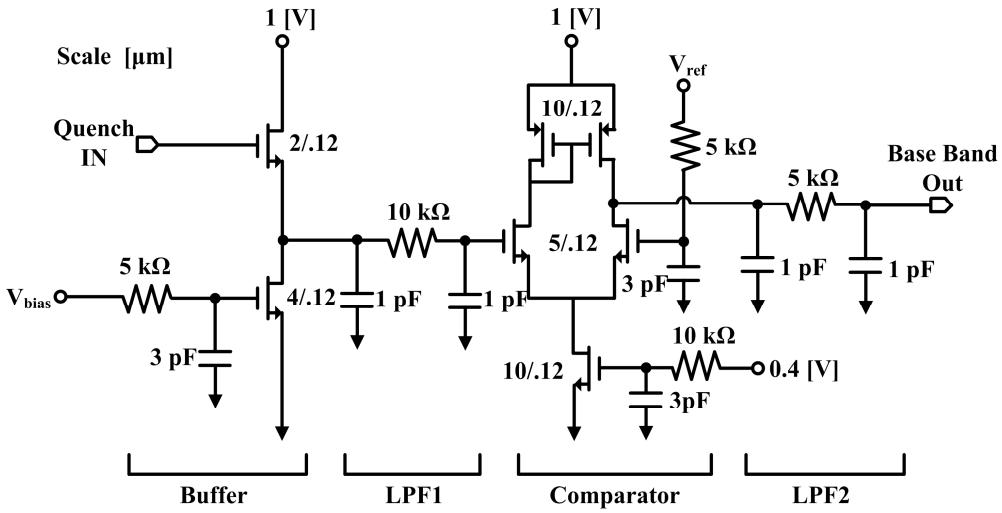

Fig. 4.11 Schematic of the active RC filter

The active RC filter is shown in Fig. 4.11. The buffer reduces the capacitive loading effect of the DSQL. Also, this structure is suitable for a low-power topology, as the buffer consumes power only when quench signal is “1”. The resistors comprising LPF1 and LPF2 are used for small size of receiver instead of inductors. The comparator is biased near sub-threshold for low idle current and compares the level of voltage delivered form the buffer and V_{ref}. Finally, the quench signals are

transferred by active RC-filter to baseband signal.

The proposed super regenerative receiver was designed for 0.13 μm CMOS technology. A 1.0 [V] DC is supplied to the overall receiver. ADS was used to design an isolation amplifier and oscillator. The digital blocks were designed with hspice. Moreover, the overall system was simulated with hspice including the boding wires at 0.4 nH at each supply and ground. The simulation results of the gain, noise figure, and input reflection characteristics of the LNA stage are shown in Fig. 4.12. The simulation results of the LNA stage were presented with a gain of 38 dB, and the NF was under 3dB at 500MHz.

For the overall system, the transient simulation is shown in Fig. 4.13. The RF power with random data was driven into the designed receiver. The injected signal had a 10 Mbps data rate and - 85 dBm power level. An input voltage wave was observed at the node of the next matching network.

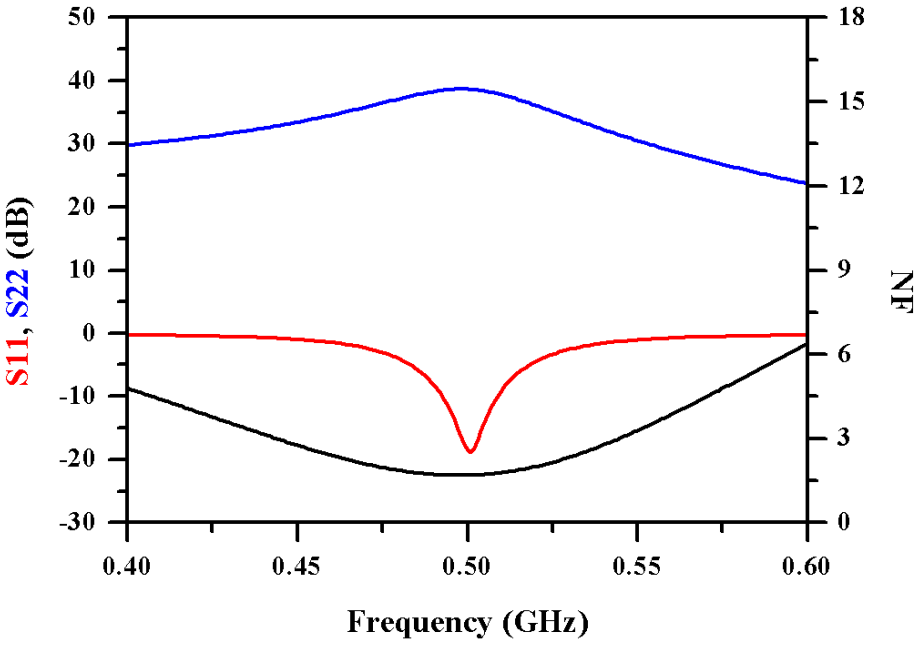

Fig. 4.12 Simulation result of LNA stage

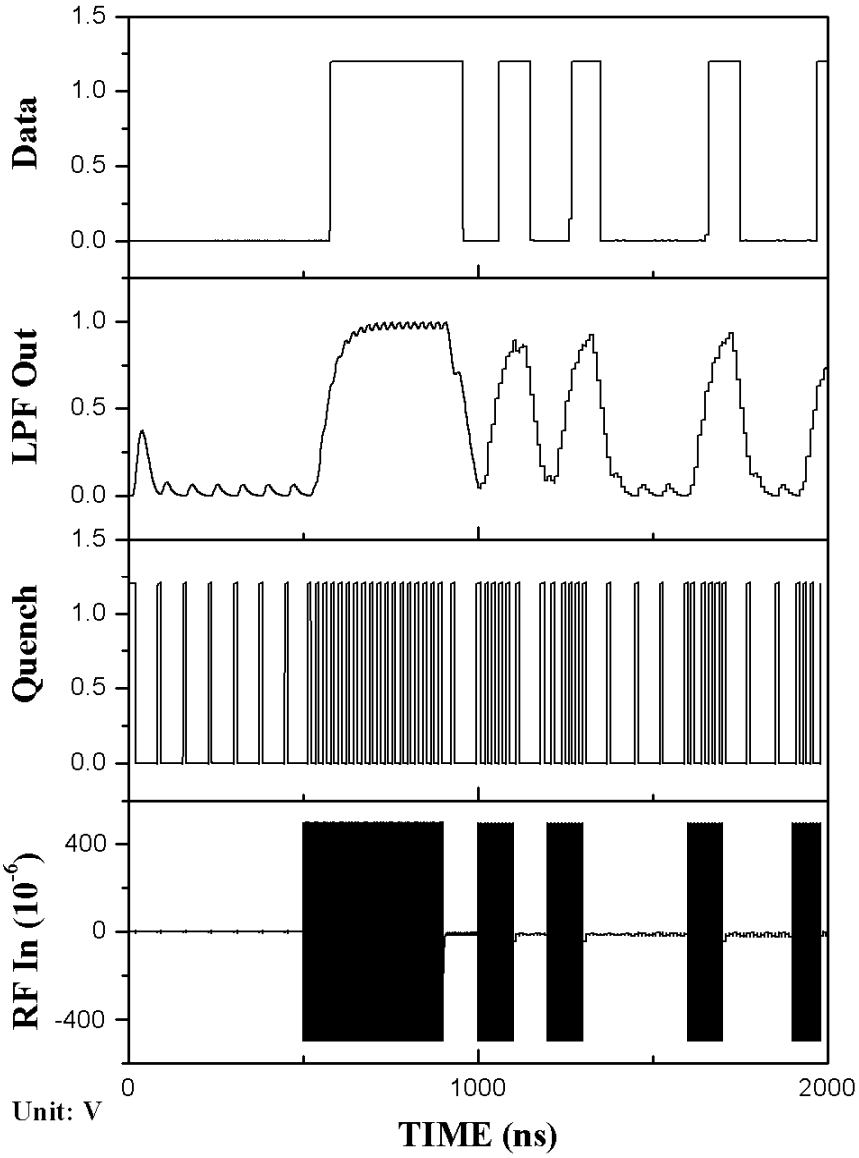

Fig. 4.13 Transient simulation of proposed receiver

4.4 Experimental results

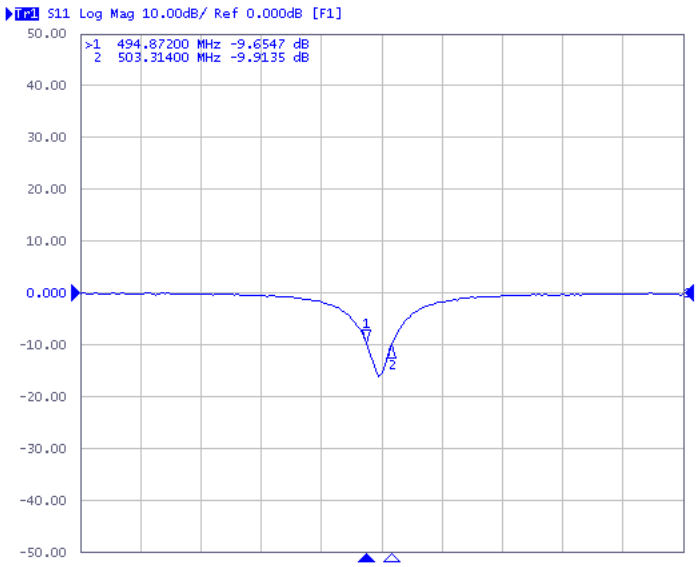

Fig. 4.14 S (1, 1) of proposed receiver

A prototype was fabricated using a 0.13-μm CMOS process according to the block diagram shown in Fig. 4.7 and Fig. 4.9. The chip size is 0.7 mm^2 including the pads. The external passive components were used in the matching network of LNA and in the inductor of the oscillator. The measured input bandwidth with -10 dB reference was 8.4 MHz that makes a small degradation of receiver's sensitivity at 10 Mbps.

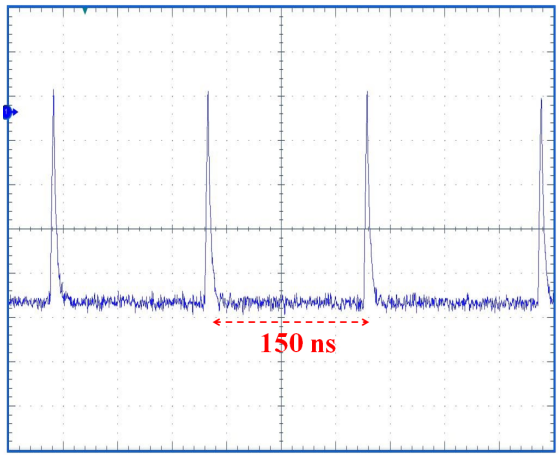

(a)

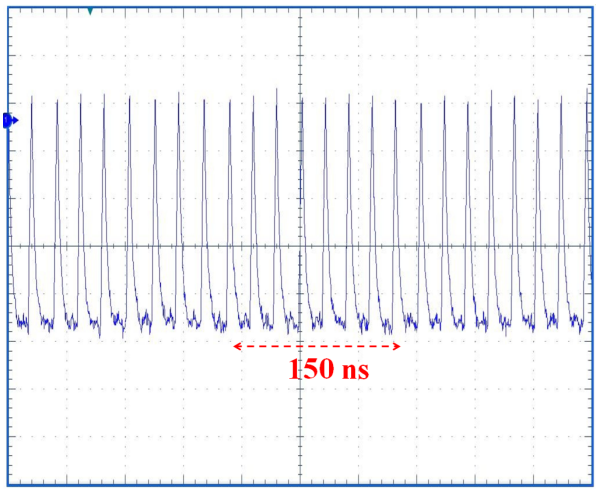

(b)

Fig. 4.15 Measured frequency variation of quench signal Q(t) in time-domain :

(a) without RF input signal and (b) with -70 dBm RF input signal

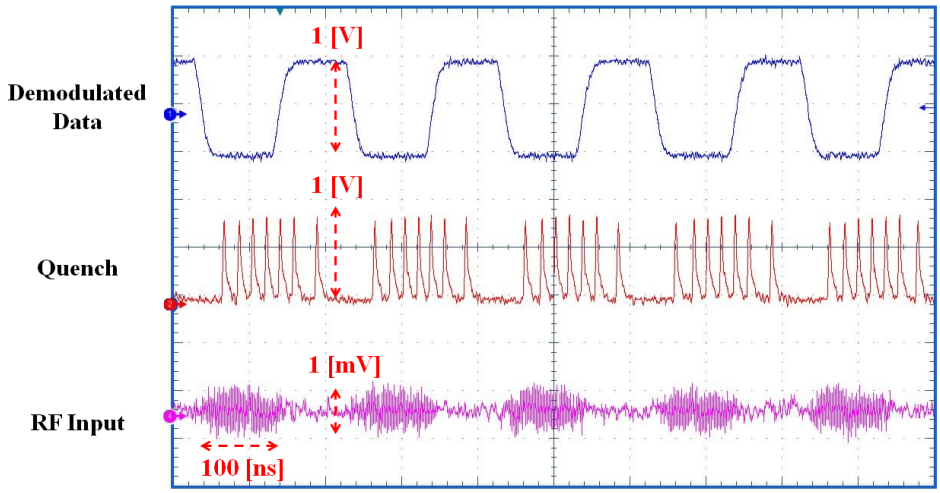

Fig. 4.16 Measured demodulated data, quench, and RF input signals at 10 Mbps in a time-domain

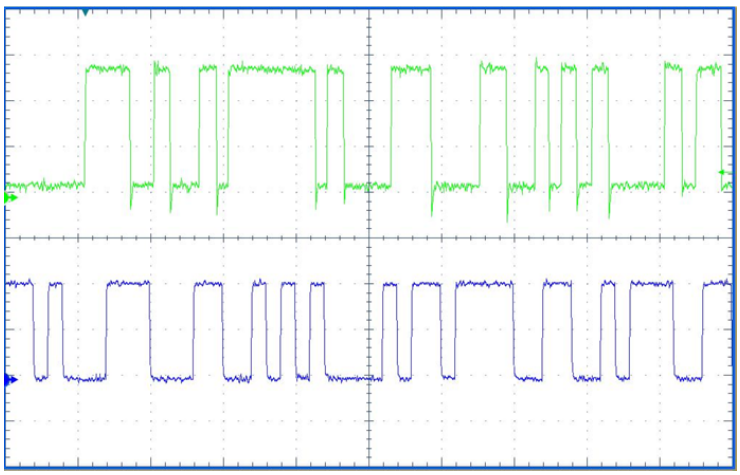

Fig. 4.17 Measured demodulated data (up) with original data (down) at 5 Mbps, -83 dBm

To verify the DSQL mechanism, the fabricated chip was tested in a time-domain using a Tektronix DPO7254 oscilloscope. When the continuous RF signal with -70 dBm was injected into the receiver, an increased quench frequency (Fig. 4.15 (b)) was generated, which was about seven times higher than the original quench frequency (Fig. 4.15 (a)). Fig. 4.16 shows the measured signals (demodulated data, quench, RF input) when the on-off keying (OOK) signal with 10 Mbps came to the receiver. The results shows that the number of quench cycles generated per received symbol is seven

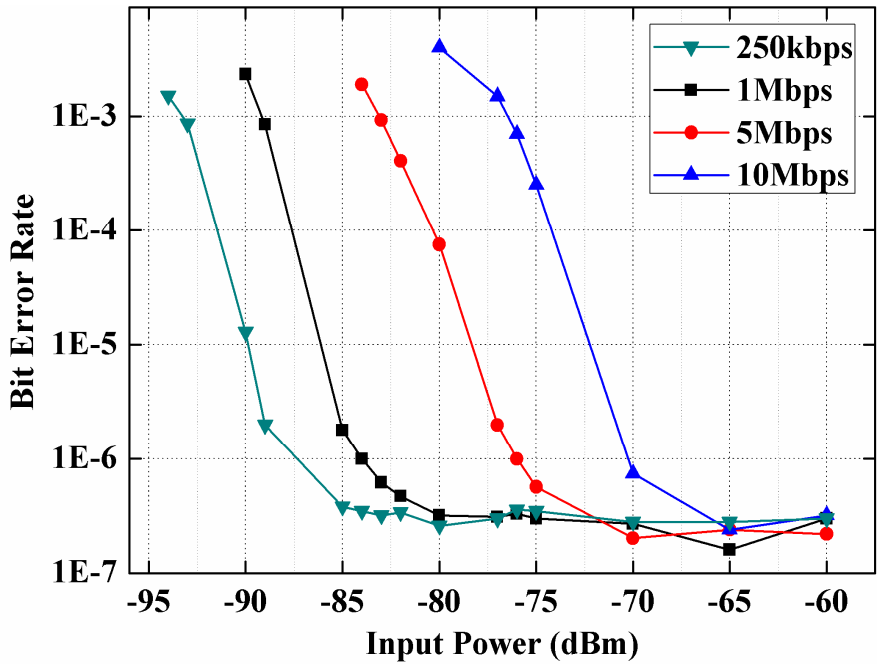

Fig. 4.18 BER measurement results of the designed receiver

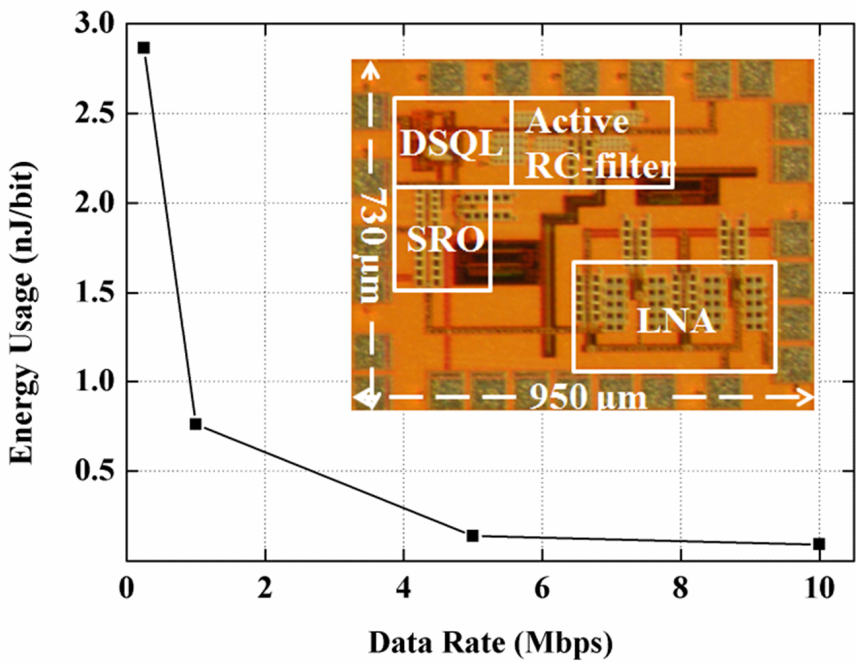

Fig. 4.19 Total energy consumption for the receiver at each data rates. A chip photo of the proposed receiver is also shown

The BER of the fabricated chip was measured using an Agilent E4438C signal generator. For this measurement, a PN23 random OOK signal with a total 10 Mbits was used. The V_{bias} value in the active RC filter was fixed at 0.3 V, while the V_{ref} value was properly biased externally. The measurement results for different data rates (250 kbps. 1 Mbps, 5 Mbps, 10 Mbps) are presented in Fig. 4.18 The sensitivity levels with BER values of 10^{-3} were -93 dBm, -89 dBm, -83 dBm, -76 dBm, respectively. Fig. 4.19 shows the total energy consumption for the receiver at each data rate. The minimum energy usage is 0.09 nJ/bit at 10 Mbps.

4.5 Summary and conclusion

Table I shows a comparison of the proposed receiver and SRRs described in a recent publications [42], [43], [47], [48]. The results show the low-power/high-data-rate characteristics of the proposed receiver.

In this letter, we propose a new type of SRR which uses a DSQL for low-power/high-data-rate applications. The designed receiver with the DSQL exhibits good sensitivity (-76 dBm), low energy usage (0.09 nJ/bit at 10 Mbps) and simplicity without an envelope detector. The experimental results show that the proposed structure is suitable for low-power medical implant applications or capsule endoscopy applications which require a high data rate.

Table 4.2 Comparison with a recent super-regenerative receiver

Parameter	[42]	[43]	[47]	[48]	This work
Tech (nm)	180	180	180	180	130
Modulation	FM-UWB	OOK	BFSK	IR-UWB	OOK
Frequency (GHz)	3.5, 4.5	0.402	2.4	3.494, 3.993	0.5
Supply (V)	1.5	1.3	0.65	1.5	1
Power Consumption (mw)	1.5	0.9	0.215	10.8	0.9
Data Rate (Mbps)	2	0.156	2	10	10
Sensitivity (dBm)	*-95	-75	-75	-66	-76
Energy (nJ/bit)	0.75	5.8	0.175	0.24	0.09

*At BER value of 10^{-6}

Chapter 5

A Transmitter with Current-Reused and Current-Combining PA

5.1 Introduction

In short-range wireless communication, especially when using medical implant application such as capsule endoscopy, an epiretinal prosthesis, a high-speed and high-efficiency transceiver is required to transmit high-resolution images for accurate diagnoses and to extend the battery life of the device [52]. Thus, a high efficiency transmitter is essential for increasing the total transceiver efficiency due to its large DC power consumption. Simultaneously, the transmitter should have enough bandwidth for a high-data- transmission rate.

An On-Off Keying (OOK) transmitter is one candidate for solving these issues in low-power applications, such as Medical Implant Communication Services (MICS) and, Wireless Sensor Networks (WSN), because of the transmitter's low-power consumption and high-data rate [51]-[54],[13].

5.1.1 Previous study of OOK transmitter

In order to design a high-efficiency transmitter, [52] used a class-B PA that has a gate bias switch to turn off the PA during Off-state and [53] used Film Bulk Acoustic Resonators (FBAR) to decrease the oscillator's power consumption. Simultaneously, [53] co-designed with the antenna whose input impedance equals optimum impedance of its power amplifier. It is no need the matching between antenna and amplifier. Therefore, the loss of inter-stage matching can be avoid and its efficiency could be better.

Other studies, [51] adopted the type of current-reused LC-oscillator employed in RF-carrier generation despite a limitation of data rate and [54] employed a complementary voltage-controlled oscillator for obtain high G_m of oscillator.

5.2 Main idea of proposed transmitter

Normally, a simple type of power amplifier with a general structure, which operates in Class B, has several problems. First, additional transistor is needed to have a switching role to modulate RF signals. This makes the limitation of data-rate due to its switching speed. And the conventional structure has intrinsically limitation on the power efficiency in low power application since the supply voltage is too high for such a low power. This type of PA should have high impedance transform ratio which results in the very narrow bandwidth. Moreover, having a low feasibility of output matching, Obtaining for high efficiency is very difficult in conventional structure.

A bandwidth of current combining structure could be better than that of conventional structure. Generally, the optimum load impedance value for maximum output power should be transformed into the antenna's input impedance. When the ratio of two impedance values is lowered, the loss of the matching circuit is reduced. The relation of the transform ratio and Quality factor (Q factor) is shown below:

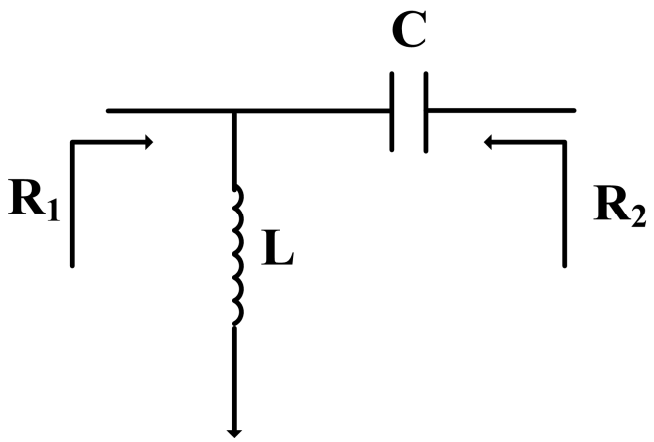

Fig. 5.1 LC matching network for impedance transform

$$Q = \sqrt{\frac{R_1}{R_2} - 1}, R_1 > R_2 \tag{5.1}$$

It is shown in the preceding equation that Q factor becomes lower if the transform ration of matching circuit becomes smaller. Furthermore, it is known that the bandwidth becomes wider in the same situation.

To lower the ratio, the current-combining structure is used. It lowers the transform ration by combining more than a couple of matching circuits in parallel, since an optimum load value is divided with the number of the composing circuits

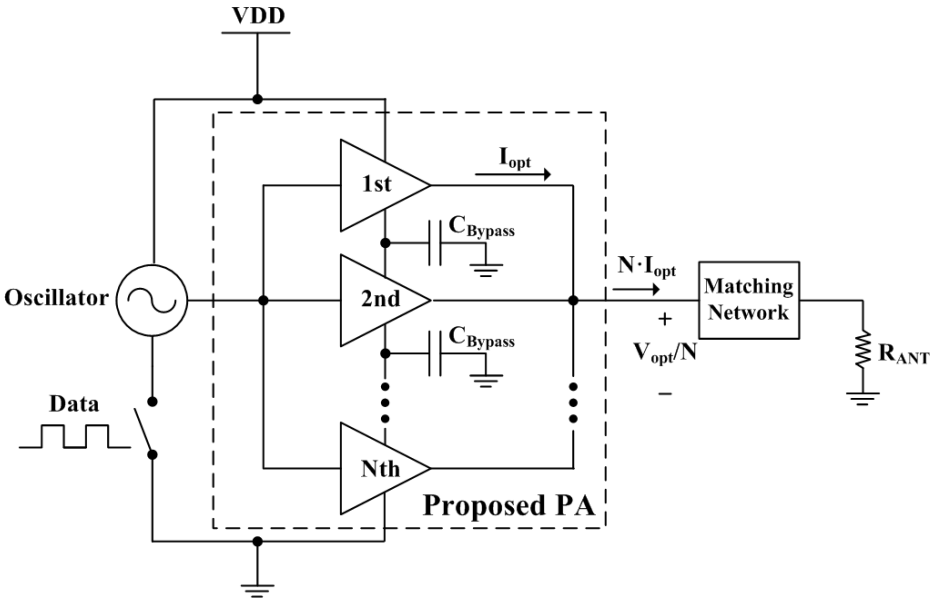

Fig. 5.2 Block diagram of the OOK transmitter with proposed PA

Fig. 5.2 shows the block diagram of OOK transmitter including the proposed power amplifier. R_{opt}, I_{opt}, V_{opt} are optimum impedance, current, and voltage of a conventional PA with a supply voltage (VDD), respectively. R_{ANT} is an antenna's input impedance.

Since the powers of the current-reuse N-power amplifiers are combined in parallel at the output node, the output voltage is lowered to one Nth of the conventional amplifier's and the amplitude of the output current is N times that of the conventional amplifier's. Therefore, the optimum impedance value of the proposed PA structure becomes $1/N^2$ times of that of a conventional type of PA structure.

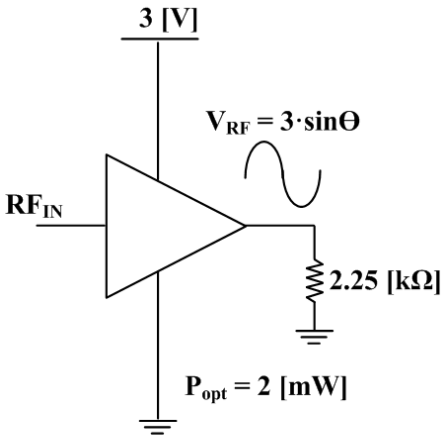

Conventional PA structure

(a)

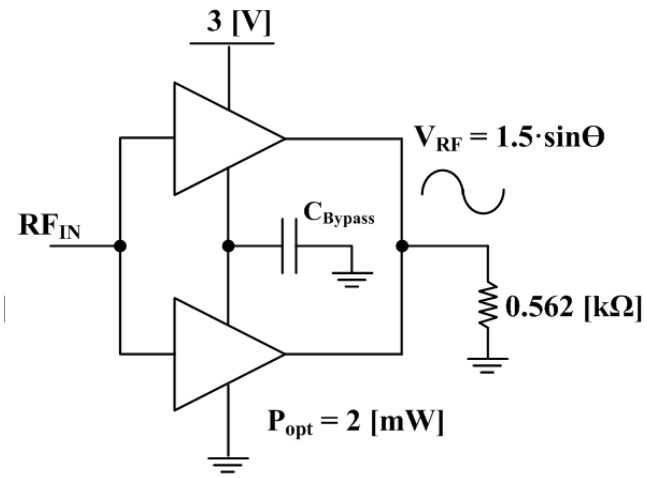

Proposed PA structure

(b)

Fig. 5.3 Example for comparing conventional PA with proposed PA

The quantitative example is shown in Fig. 5.3. The optimum impedance of a conventional PA for 2 mW of output power with 3 V supply voltage is 2.25 kΩ without considering the knee voltage. The optimum impedance of the proposed PA, whose N equals two, is about 0.562 kΩ under the same conditions. Thus, the output matching circuit of the proposed PA has to transform 0.562 kΩ into the antenna's impedance. The example suggests that the proposed PA has an inherently lower matching loss and wider bandwidth than a conventional PA.

In this study, we design the OOK transmitter integrated with the high-efficiency wideband PA proposed [55], [56] in detail and show the measurement results of the fabricated chip. The proposed PA that operates in Class C employs a bias current-reused and RF current-combining structure, which decreases the optimum-load impedance so that the loss of matching circuit is reduced and the bandwidth of the PA is widened. Also, the current-reused type is suitable for low-power applications [51]. Therefore, the transmitter's bandwidth and efficiency are maximized.

The operating frequency and the target output power are set to 500 MHz and 0 dBm respectively from previous work [52]. The fabricated PA shows a maximum drain efficiency of 59.5 % at 500 MHz with 1.62 dBm output power, while the measured efficiency of the transmitter is 44.9% during On-state. The efficiency of transmitter is 38.4% and the energy usage is 22 pJ/bit at 100 Mbps with -0.75 dBm

average output power.

5.3 Description of proposed transmitter

5.3.1 Current-combining and current-reused PA

Fig. 5.4 shows the schematic of the PA, which consists of two-amplifier units employing a current-combining and current-reused structure. The 2-stack is chosen for minimizing the number of external components and a knee voltage effect at 3 V supply voltage. A knee voltage limits the voltage swing of PA [57]. The proposed PA is biased Class C, which has a high efficiency due to its low conduction angle and zero idle current without using a gate bias switch. The external inductor of 130 nH (LQW18ANR13G00) and output capacitor of 1 pF (GRM1555C1H1R0CZ01) transform the optimum load impedance (1.125 kΩ) into twice that of the antenna's input impedance (0.4 kΩ) in a single amplifier. These passive components are a choke inductor and a DC block capacitor, respectively, in the ideal case shown in Fig. 5.3.

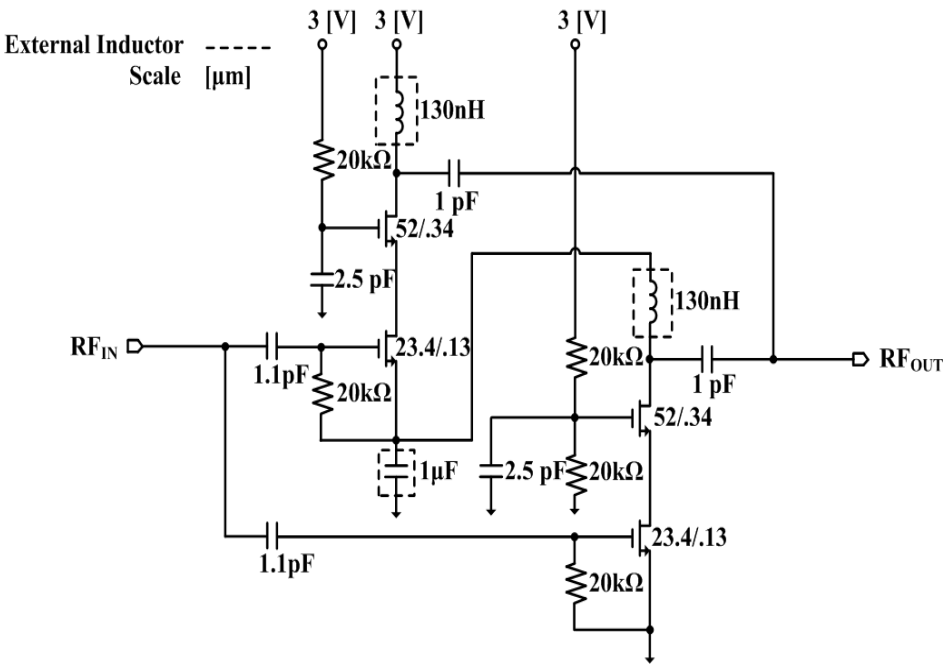

Fig. 5.4 Schematics of proposed PA comprised of two amplifier units

In non-ideal case, a knee voltage (V_{knee}) limits the voltage swing of PA [57]. In case of N-stacked proposed PA, the total voltage swing is reduced to (2VDD/N-V_{knee}) under the same condition (output power, the supply voltage) for the conventional PA such as Fig. 5.5. Therefore, the number of stacked PA could be limited at fixed supply voltage condition. Also, the number of external components (C_{bypass}) is proportional to N in this work.

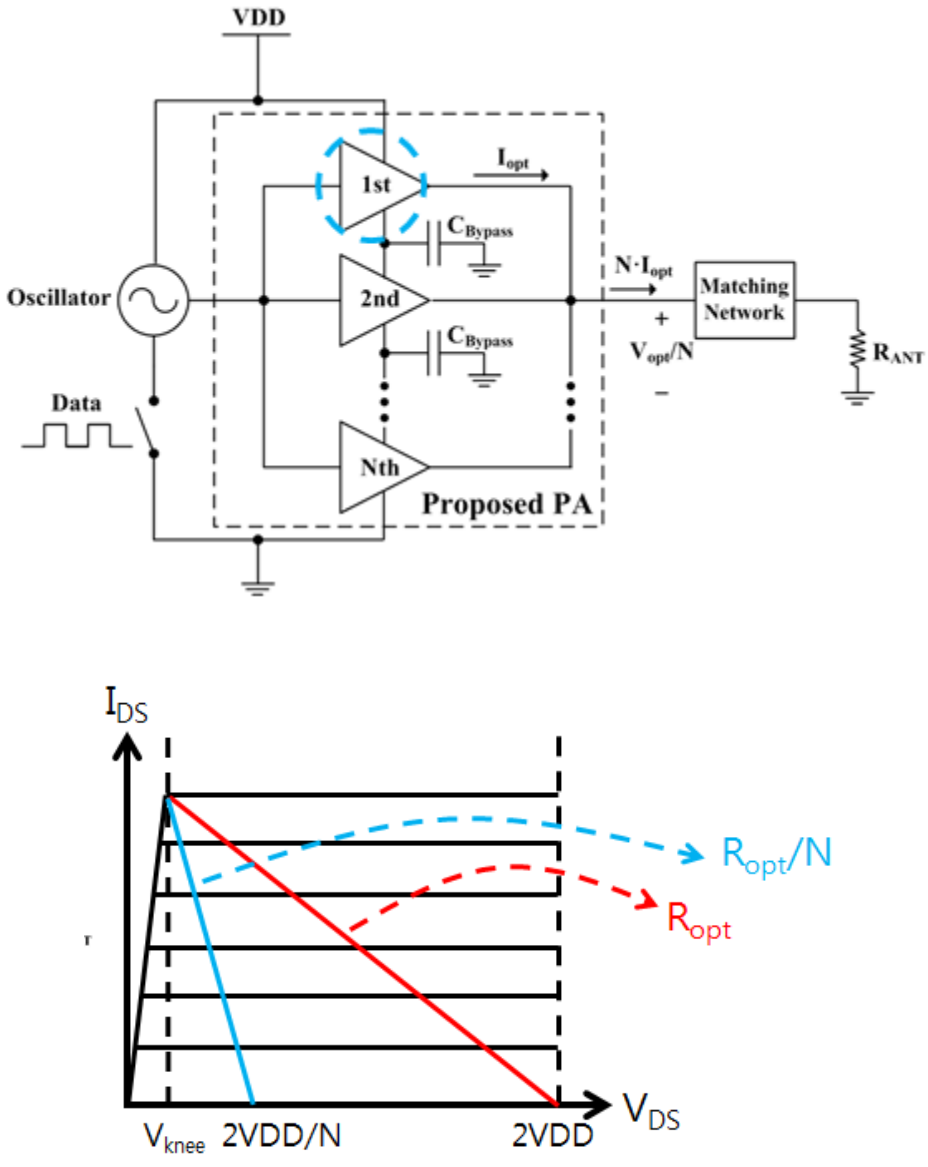

Fig. 5.5 Load line graphs of conventional and proposed PAs

5.3.2 Ring oscillator with driving buffer

A ring-type oscillator is adopted for this work, since a ring oscillator has faster start-up time than an LC oscillator [37], making it suitable for a high-speed OOK modulator. Moreover, the frequency stability exhibited by ring oscillator will suffice in the human body, maintaining a constant temperature. Fig. 5.6 shows the schematic of ring oscillator including buffers to deliver an RF signal to the PA input. The size of buffers is carefully chosen for driving a signal to PA. The NAND gate switch is adopted for OOK modulation and its oscillation frequency is tuned by V_{freq} bias with transistor size selection. The supply voltage of 1.9 V is used to limit the input voltage swing of the PA stage and its time period from start-up to steady state is 1.5 ns in simulation shown Fig. 5.7.

The narrow-pulsed input-waveform of the PA makes the PA operation in deep class C. Because, the conduction angle of PA is reduced by sharped input-waveform. Therefore, the size of buffer for driving PA is adjusted for shaping the sharp waveform of input voltage.

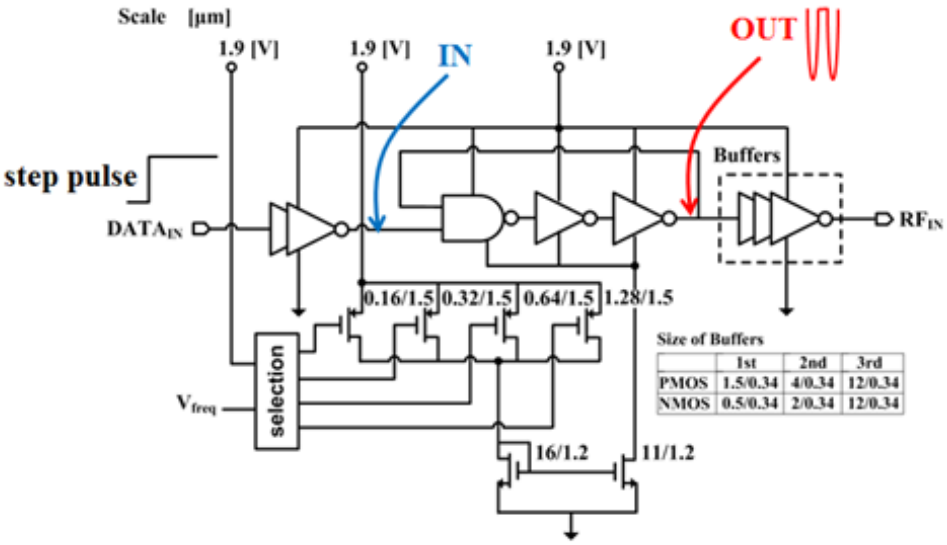

Fig. 5.6 Schematic of ring oscillator with driving buffer

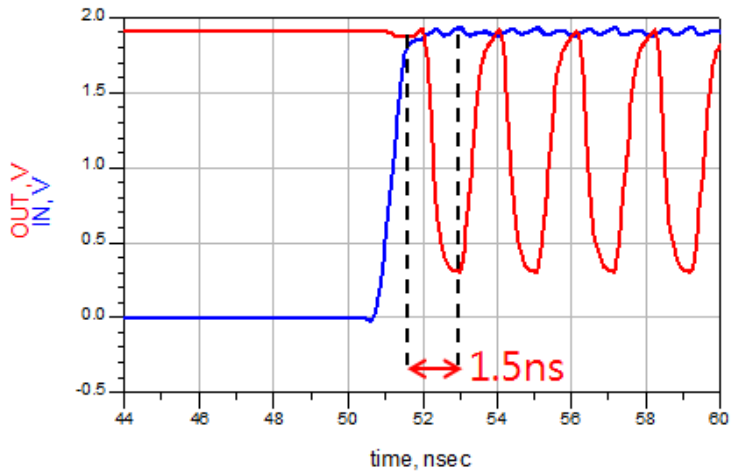

Fig. 5.7 Simulated time period of ring oscillator from start-up to steady state

5.4 Experimental results

A prototype was fabricated using a 0.13-μm CMOS process in the block diagram shown in Fig. 5.2. The chip size is about 0.6 mm^2 including the pads. For the test, an additional matching circuit between the spectrum analyzer and transmitter was used to transform 50 Ω into 200 Ω, because the PA was designed for the antenna's input impedance of 200 Ω.

To verify the proposed PA performance, the PA stage was tested in a frequency domain using an Agilent N9020A spectrum analyzer. The output power and its drain efficiency were measured without an input-matching circuit, because a ring oscillator practically delivers the voltage signal to the PA. When the continuous RF signal with 3 dBm was injected into the PA, the measurement results are shown in Fig. 5.8. The variation of the output power is less than 3dB and the efficiency exceeds 40 % in the 450-550 MHz range. The maximum efficiency was 59.5 % at 500 MHz with 1.62 dBm output power

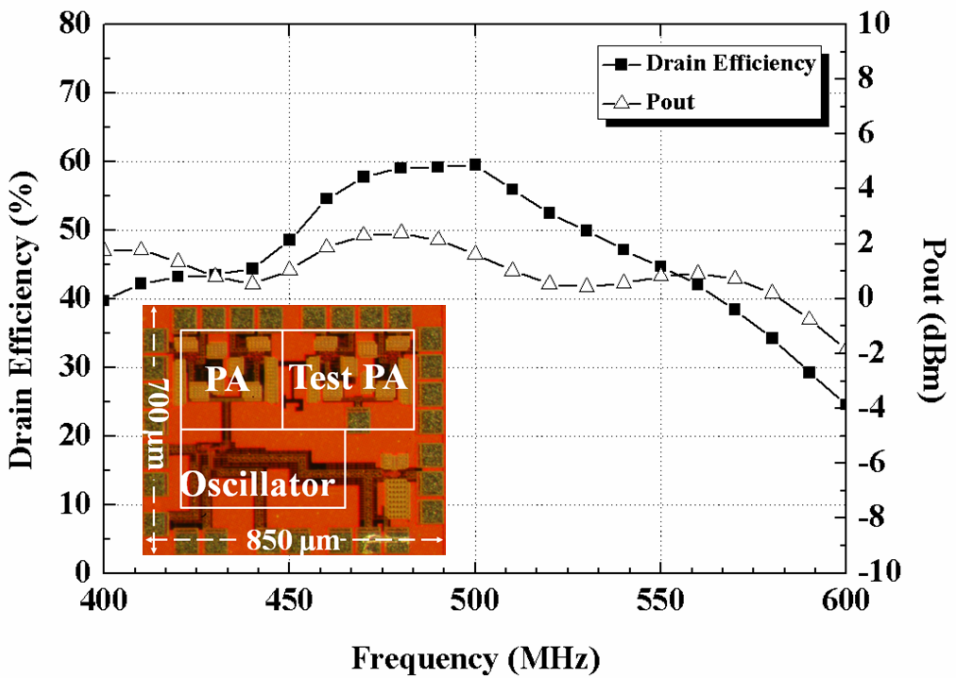

Fig. 5.8 Measured drain efficiency and output power of proposed power amplifier. A chip photo of the designed transmitter is also shown

The transmitter including a ring oscillator was measured to verify the overall performance of the designed OOK transmitter. The total efficiency of the transmitter at 500 MHz was 44.9 % with 1.62 dBm output power during the On-state. Fig. 5.9 shows the measured frequency domain output spectrum during the On-state (a) and the modulated power stated (b) with 100 Mbps data rate. The time-domain OOK signal with '1010' data at 100 Mbps rate is shown in Fig. 5.10, which shows the falling and rising time of around 2 ns. And, the transmitter's frequency error caused by the frequency drift is 0.058 % shown in Fig. 5.11.

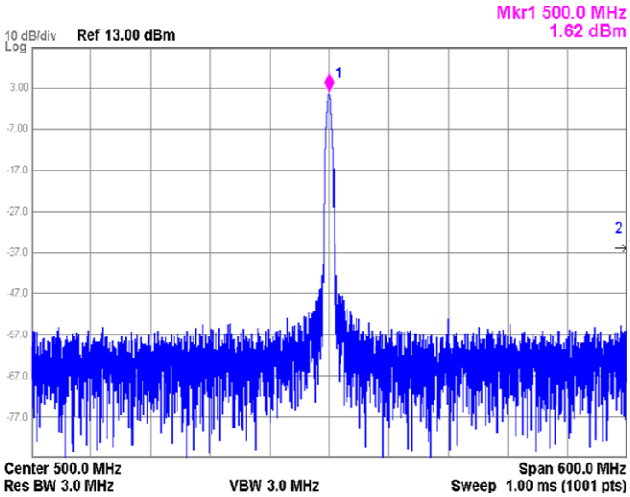

(a)

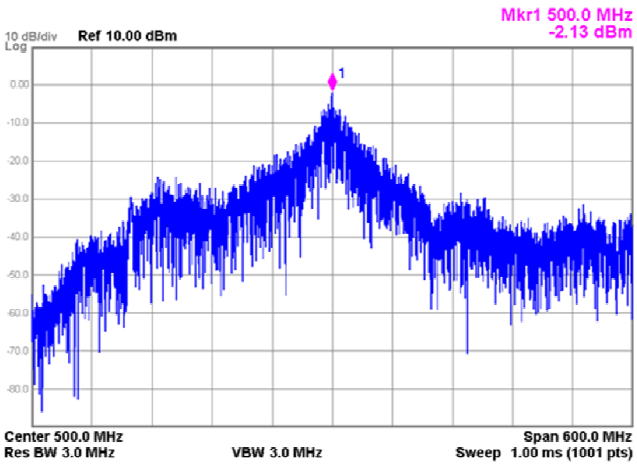

(b)

Fig. 5.9 Measured output spectrum of PA under the continuous power state (a) and modulated power state (b) with 100 Mbps data-rate of PRBS pattern

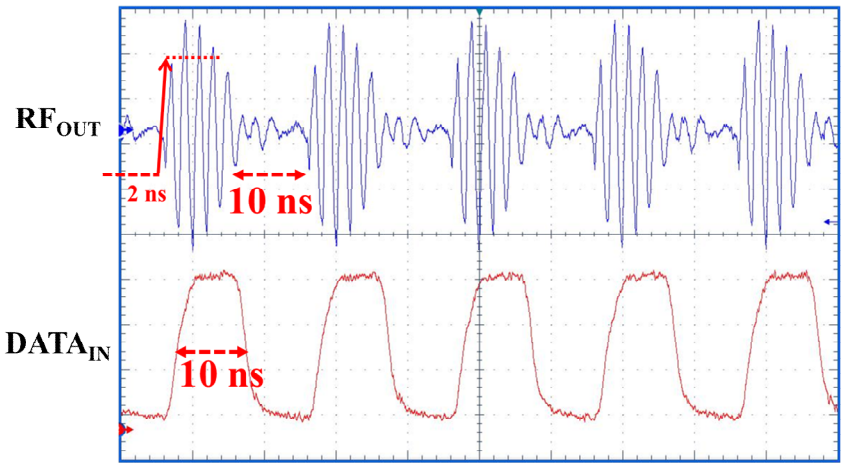

Fig. 5.10 Measured time-domain output signal of transmitter with '1010' data at 100 Mbps

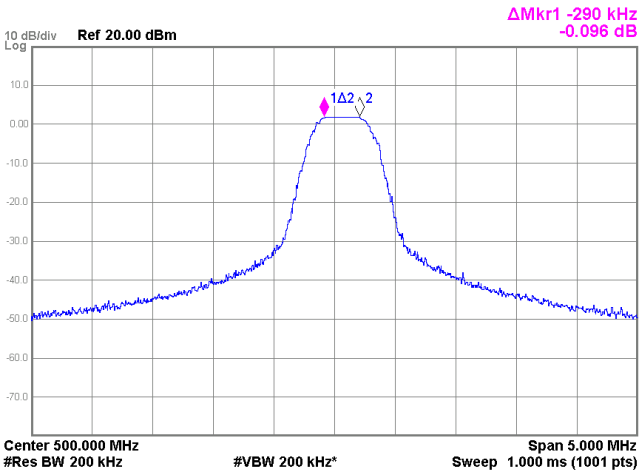

Fig. 5.11 Measured frequency drift of proposed transmitter

When the transmitter is in the On-Off state, the modulation makes the power spread within a certain frequency range. Therefore, the average power was measured with the channel bandwidth of each data rate. Fig. 5.12 shows the results of the measured average power and efficiency, and energy usage at each data rate of Pseudo Random Binary Sequence (PRBS). The maximum efficiency is 38.4% and the minimum energy usage is 22 pJ/bit at 100 Mbps data-rate with -0.75 dBm output power. The self-biasing effect of an OOK modulated pulse input to the gate of PA causes the more output power than that expected, -3dB. This effect can checked through the ADS transient simulation shown in Fig. 5.13. The bias level of PA effectively increased, when the pulse input signal come to the input of PA. The bias level of PA is unstable in low power application due to high bias resistor, which protects transistor from breakdown by static charge and prevent leakage power toward bias path.

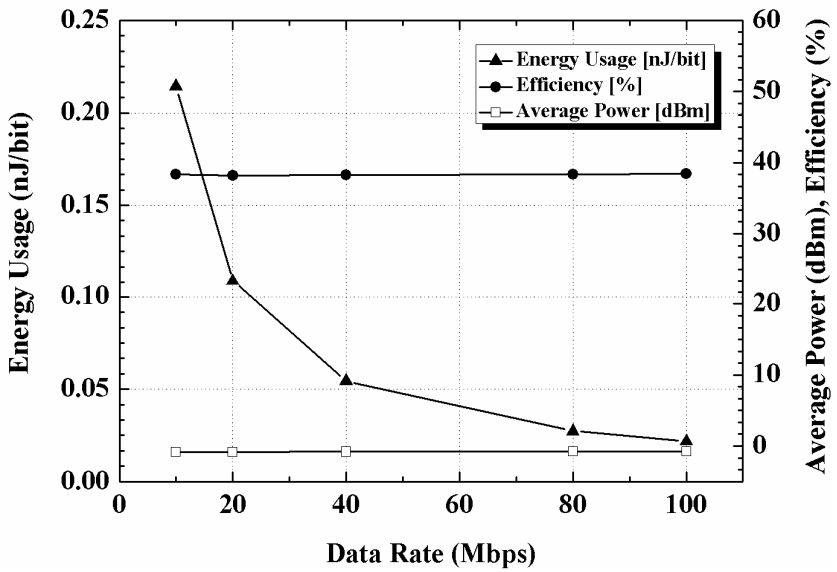

Fig. 5.12 Measured efficiency and average output power, energy usage of transmitter at each data rates with PRBS pattern

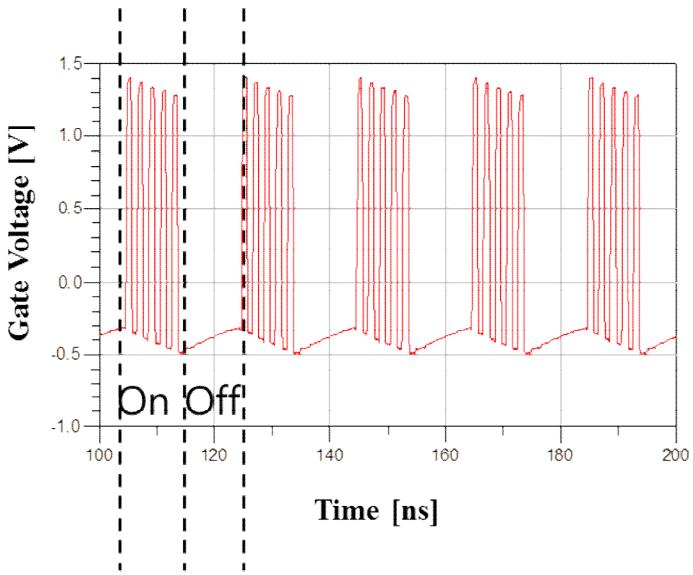

Fig. 5.13 ADS simulation results at gate with modulated signal

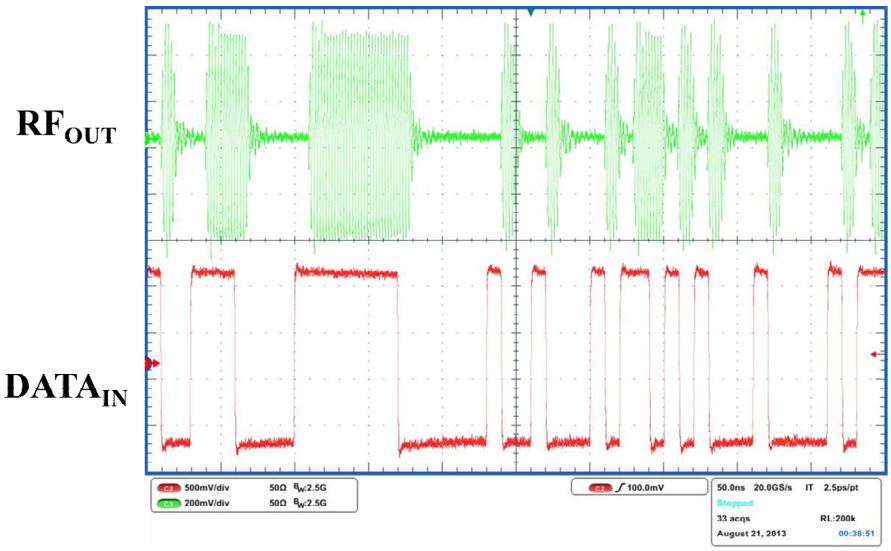

Fig. 5.14 Measured time-domain signal at transmitter's output with PRBS data (100 Mbps)

5.4 Summary and conclusion

Table 5.1 shows a comparison of the designed transmitter and the OOK transmitters described in publications [13], [51]-[54]. The results show the low-power/high-data-rate characteristics of the designed transmitter.

In this work, we propose an OOK transmitter with a high efficiency wideband PA that employs a current-reused and RF current-combining structure for low-power/high-data rate applications. The designed transmitter exhibits good efficiency (38.4%) and, low energy usage (22 pJ/bit) at 100 Mbps. The experimental results show that the designed transmitter is suitable for low-power medical implant applications or capsule endoscopy applications, which require high speed and efficiency.

Table 5.1 Comparison with OOK transmitter

Parameter	[52]	[53]	[51]	[13]	[54]	This work
Tech (nm)	130	130	180	90	40	130
Method	Class-B & Bias Switch	FBAR VCO	[1]CR VCO	Pulse Shape	[2]C-VCO	[3]CRCC PA
Freq. (GHz)	0.5	1.9	0.44	2.4	2.4	0.5
VDD (V)	3.1	0.65	3	1	1.5	[4]3, 1.9
Data Rate (Mbps)	20	0.33	40	10	136	100
DC Power (mW)	2.53	1.35	2.58	2.3	3	2.19
Modulated Output Power (mW)	0.7	1.2	[5]0.48	1	0.04	0.84
Efficiency (%)	27.7	46	18.6	26	1.3	38.4
Energy Usage (pj/bit)	126.5	409	64.5	23	22	0.09
[6]FOM (pj/bit/mW)	180.7	341	134	230	550	26

[1]Current Reused Voltage Controlled Oscillator (VCO), 2Complementry-VCO.

[3]Current Reused and Current Combining PA.

[4]VDD of PA: 3 V, VDD of ring oscillator: 1.9 V.

[5]Assuemd Modulated Output Power = On-time Output Power [51] /2.

[6]FOM = Energy Usage / Output Power [13].

Chapter6

Conclusion

In this thesis, the design method and structure for medical implant application was proposed to solve low power and high data-rate. At first, the propagation loss was calculated based on FCC muscle model and a capsule system is designed for verifying the analysis of results. The designed system was fabricated as CMOS process and the image recovered in liquid phantom and pig successfully. These results show that the calculated frequency is suitable for medical implant application.

Secondly, we proposed a new type of SRR which uses a DSQL for low-power/high-data-rate applications. The designed receiver with the DSQL exhibits good sensitivity (-76 dBm), low energy usage (0.09 nJ/bit at 10 Mbps) and simplicity without an envelope detector. The experimental results show that the proposed structure is suitable for low-power medical implant applications or capsule endoscopy applications which require a high data rate.

Lastly, we suggested an OOK transmitter with a high efficiency wideband PA

that employs a current-reused and RF current-combining structure for low-power/high-data rate applications. The designed transmitter exhibits good efficiency (38.4%) and, low energy usage (22 pJ/bit) at 100 Mbps. The experimental results show that the designed transmitter is suitable for low-power medical implant applications or capsule endoscopy applications, which require high speed and efficiency.

Chapter7

Appendix

7.1 Output spectrum of OOK signal

For the verifying the data rate of the proposed transmitter at chapter 5, the theory of furrier series can help. In ideal case, the CW-pulse train can be presented as sinc-function at frequency-domain, which is the well-known fact in radar application. And its center frequency is determined by CW frequency. In OOK application, the CW generated by ring-oscillator has a harmonic component. Therefore, the spectrum of OOK signal can be shown as Fig 7.1 (a). Also, the measurement result shows same spectrum shape in frequency domain as Fig 7.1 (b). These results can prove the operation of proposed OOK transmitter with 100 Mbps not using BER test of receiver for demodulation..

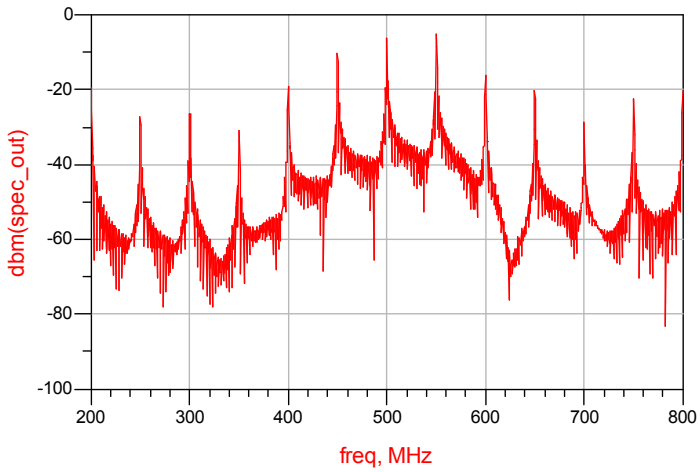

(a)

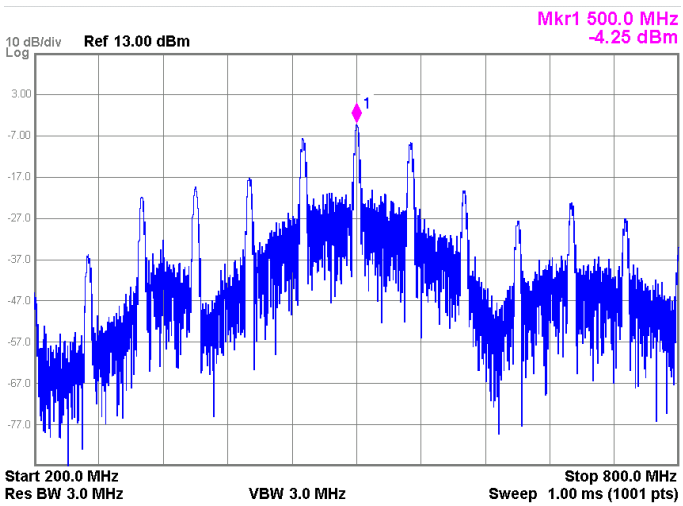

(b)

Fig. 7.1 Simulated output spectrum of transmitter (a) and measure output spectrum of transmitter with 100 Mbps data-rate of '1010' pattern

7.2 The theoretical BER of OOK comunication

For comparison of BER test results at chapter 4 with the theoretical BER of OOK, the BER versus input power can be calculated using communication system theory [58]. About non-coherent receiver, probability error, bit-error-rate, can be presented as follow equation:

$$P_e = \frac{1}{2}\left[P_{eS} + P_{eM}\right] \tag{7.1}$$

$$P_{eS} = 1 - Q\left(\sqrt{2E_b / N_0}, \sqrt{2 + E_b / 2N_0}\right) \tag{7.2}$$

$$P_{eM} = \exp\left(-\frac{2 + E_b / 2N_0}{2}\right) \tag{7.3}$$

$$\frac{E_b}{N_0} = \frac{Input - Power}{kT \cdot (Data - Rate)} \tag{7.4}$$

And, Q () is the Marcum-Q function. k is Boltzmann constant. T is Kelvin temperature (300 K). The calculated results is shown as Fig 7.2

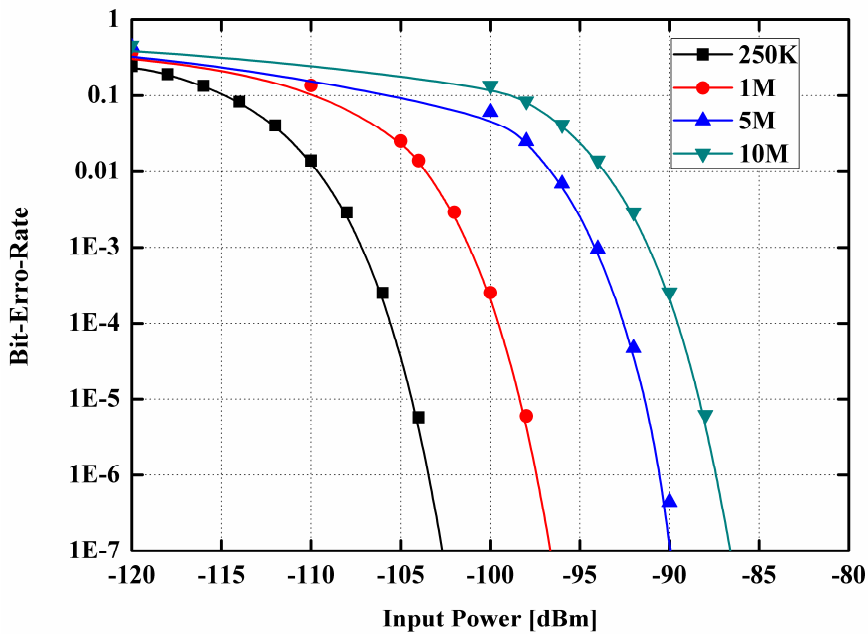

Fig. 7.2 Calculated results of theoretical BER of OOK communication

Bibliography

[1] H. Li *et al.*, "Trend and standardization of Body Area Network for Medical Healthcare," in *Proc. the 1st European Wireless Technology Conference*, pp.1-4, 2008.

[2] J. Choi *et al.*, "A study in the wireless Body Area Network Applications and Channel Models," in *Proc. the 2nd international Conference on Future Generation Communication and Networking*, pp.263-266,2008.

[3] Y. Hao and R. Foster, "Wireless body sensor network for health-monitoring application," *Physiological* Measurement, 29, R27-R56, 2008.

[4] H. S. Nam, H. S. Lee and J. Y. Kim, "Trend of WBAN Application," *Electronic and Telecommunication Trends*, vol. 24, no.5, pp. 109-118, 2009.

[5] Guido Dolmans, "Applications, Channels, and Radio Architectures", *IEEE* P802.15-08-0163-00-0006.

[6] G. Iddan, G. Meron, A. Glukhovsky, *et al*, "Wireless capsule endoscopy" in Nature, vol.405, pp.417-418, May 2000.

[7] P. Quinlan *et al*., "A multimode 0.3-200-kb/s transceiver for the 433/868/915-MHz bands in 0.25-/spl mu/m CMOS." *IEEE J. Solid-State-Circuits*, vol. 39, no. 12, pp. 2297-2310, Dec. 2004.

[8] A. Fakher, M. J. Deen, and H. deBruin, "Low-voltage, low-power and low phase noise 2.4GHz VCO for medical wireless telemetry, " *in Proc. Can. Conf. Electrical and Computer Engineering*, vol.3, pp. 1321-1324, May 2004.

[9] P. M. Izdebski, H. Rajagoplan, and Y. Rahmat-Samii, "Conformal ingestible capsule antenna: A novel Chandelier meandered design, " *IEEE Trans. Antennas Propag*., vol. 57, no. 4, pp. 900-909, Apr. 2009.

[10] K. Chen, Z. Yang, L. Hoang, J. Weiland, M. Humayun, and W. Liu, "An integrated 256-channel epiretinal prosthesis, " *IEEE J. Solid-State Circuits*, vol. 45, no. 9, pp. 1946–1956, Sep. 2010.

[11] R.L. Schneider, N. Najafi, and D.J. Goetzinger, *Anchor for medical Implant Placement and Method of Manufacture*. Ypsilant, MI:Integrated Sensing System, Inc., 2008.

[12] E. Y. Chow, Y. A. L. Chlebowski, S. Chakraborty, W. J. Chappell, and P. P. Irazoqui, "Fully Wireless Implantable Cardiovascular Pressure Monitor Integrated with a Medical Stent, " *IEEE Trans. Biomed. Eng.*, vol. 57, no. 6, pp.1487-1496, June. 2010.

[13] X. Huang *et al.*, "A 0dBm 10Mbps 2.4GHz ultra-low power ASK/OOK transmitter with digital pulse-shaping," *in Proc. IEEE RFIC Symp. Dig.*, 2010, pp.263-266.

[14] Federal Communications commission, "Body Tissue Dielectric Parameters" 2014 [Online]. Available: http://transition.fcc.gov/oet/rfsafety/dielectric.html

[15] D. K. Cheng, "Field and Wave Electromagnetics", *2nd ed, Addsion wesley,* 1989.

[16] H.T. Friss, "A Note on a simple Transmission Formula*," IEEE Trans. Proc. IRE., vol. 34, no. 5*, pp. 254–256, May. 1964.

[17] C. Balanis, "Antenna Theory*", 3rd ed, Wiley*, 2005.

[18] S. Yun, K. Kim and S. Nam, "Outer Wall Loop Antenna for Ultra Wideband Capsule Endoscope System," *IEEE Antennas and Wireless Propagation Letters, vol.9*, pp 1135-1138, Dec. 2010.

[19] A. Karlsson, "Physical limitations of antennas in a lossy medium," *IEEE Trans, Antennas Propa., vol. 52*, no.8, pp. 2027-2033, Aug. 2004.

[20] J. Lee, , S. Nam, "Q evaluation of small insulated antennas in a lossy medium and practical radiation efficiency estimation," *in Proc. Kor. Jap. Microw. Conf.*, pp. 65-68, Nov. 2007.

[21] B. Chi, J. Yao, S. Han et al., "A 2.4GHz Low Power Wireless Transceiver Analog Front-End for Endoscopy Capsule System," *in Proc. IEEE Int. Symp. Circuits Syst.*, pp. 4907-4910, May 2006.

[22] B. Chi, J. Yao, S. Han et al., "A 2.4GHz Low Power Wireless Transceiver Analog Front-End for Endoscopy Capsule System," *in Proc. IEEE Int. Symp. Circuits Syst.*, pp. 4907-4910, May 2006.

[23] A. Glukhovsky, "Wireless capsule endoscopy," *Sensor Rev., vol.23*, no.2, pp. 128-133, 2003.

[24] L. Wang, T. D. Drysdale, and D. R. S. Cumming, “In situ characterization of two wireless transmission schemes for ingestible capsules,” *IEEE Trans. Biomed. Eng., vol. 54*, no. 11, pp. 2020-2027, Nov. 2007.

[25] S. Lee, J. Lee, Y. Yoon, S. Park “A Wideband Spiral Antenna for Ingestible Capsule Endoscope Systems: Experimental Results in a Human Phantom and a Pig,” *Trans. Biomed. Eng., vol.58*, NO.6, pp.1734-1741, June 2011.

[26] F. Carpi, S. Galbiati, and A. Carpi, “Controlled navigation of endoscopic capsules: Concept and preliminary experimental investigations,” *IEEE Trans. Biomed. Eng., vol. 54*, no. 11, pp. 2028–2036, Nov. 2007.

[27] H. M. Kim, S. Yang, J. Kim, S. Park, J. H. Cho, J. Y. Park, T. S. Kim, E.-S. Yoon, S. Y. Song, and S. Bang, “Active locomotion of a paddling-based capsule endoscope in an in vitro and in vivo experiment (with videos),” *Gastrointestinal Endoscopy, vol. 72*, no. 2, pp. 381–387, 2010.

[28] B. Chi, J.Yao, S.Han,X.Xie, G. Li, and Z.Wang, “Low-power transceiver analog front-end circuits for bidirectional high data rate wireless telemetry in medical endoscopy applications,” *IEEE Trans. Biomed. Eng., vol. 54*, no. 7, pp. 1291–1299, Jul. 2007.

[29] S. Itoh, S. Kawahito, and S. Terakawa, “A 2.6 mW 2fps QVGA CMOS one-chip wireless camera with digital image transmission function for capsule endoscopes,” *in Proc. IEEE Int. Symp. Circuits Syst.*, pp. 3353–3356, May 2006.

[30] B. Peter. (2006, July.). *RF Integrated Circuits for Medical Implants: Meeting the Challenge of Ultra Low Power Communication* [Online]. Available: http://www.cmoset.com/uploads/Peter_Bradley.pdf

[31] Toumaz UK Ltd. *Sensium Life Platform Product Brief TZ2050* [Online]. Available: http://www.toumaz.com/uploadsv3/wysiwyg_editor/files/TZ205000-MPB%20Product%20brief%20Sensium%20Life%20Platform%20V1_2.pdf

[32] Y. Gao, Y. Zheng, S. Diao, W. Toh, C. Ang, M. Je, and C. Heng, "Low Power Ultra-wideband Wireless Telemetry Transceiver for Medical Sensor Applications" *IEEE Trans. Biomed. Eng., vol. 58*, no. 3, pp. 1291–1299, March. 2011.

[33] J. Thon´e, S. Radiom, D. Turgis, R. Carta, G. Gielen, and R. Puers, "Design of a 2 Mbps FSK near-field transmitter for wireless capsule endoscopy," *Sens. Actuators, A: Phys., vol 156*, no. 1, pp. 43–48, Nov. 2009.

[34] S. I. Kwak, K. Chang, and Y. J. Yoon, "The helical antenna for the capsule endoscope system," *in Proc. IEEE Antennas Propag. Symp., vol. 2B*, pp. 804–807, Jul. 2005.

[35] S. I. Kwak, K. Chang, and Y. J. Yoon, "Small spiral antenna for wideband capsule endoscope system," *Electron. Lett., vol. 42*, no. 23, pp. 1328–1329, Nov. 2006.

[36] K. Kim, S. Lee, E. Cho, J. Choi, and S. Nam, "Design of OOK system for

wireless capsule endoscopy," *in Proc. IEEE Int. Symp. Circuits Syst.*, pp. 1205–1208, May 2010.

[37] T. Miyazaki, M. Hashimoto, H. Onodera, "A performance comparison of PLLs for clock generation using ring oscillator VCO and LC oscillator in a digital CMOS process" *in Proc. IEEE ASP-DAC*, pp.545-546., 2004

[38] H. Park, S. Lee and S. Nam, "An Inductorless CMOS 0.1-1GHz Automatic Gain Control Circuit," *in Proc. Eur. Microw, Conf.*, Oct. 2008.

[39] S. Lee, J. Lee, Y. Yoon, S. Park "A Wideband Spiral Antenna for Ingestible Capsule Endoscope Systems: Experimental Results in a Human Phantom and a Pig," *Trans. Biomed. Eng., vol.58*, NO.6, pp.1734-1741, June 2011.

[40] S. Park, J. Lee, Y. Chung, and C. Cheon, "Design of the buffer layer and absorber for enhancement of receiving sensitivity for wireless endoscopy," *in Proc. IEEE Antennas Propag. Symp*, pp. 1–4, June 2009.

[41] T. H. Lee, The design of CMOS radio-frequency integrated circuits, *2nd ed. Cambridge, UK: Cambridge University Press*, 2004.

[42] M. Anis, M. Ortmanns, N. Wehn, "A 2.5mW 2Mb/s fully integrated impulse-FM-UWB transceiver in 0.18um CMOS," *Microwave Symposium Digest (MTT), 2011 IEEE MTT-S International*, pp.1, 5-10 June 2011.

[43] Y.-H. Liu, H.-H. Liu, and T.-H. Lin, "A super-regenerative ASK receiver with DELSIG pulse-width digitizer and SAR-based fast frequency calibration for

MICS applications," *in Proc. IEEE Symp. VLSI Circuits*, Jun. 2009, pp. 38–39.

[44] J.-Y. Chen, M. P. Flynn, and J. P. Hayes, "A fully integrated auto-calibrated super-regenerative receiver in 0.13-μm CMOS," *IEEE J. Solid-State Circuits, vol. 42*, no. 9, pp. 1976–1985, Sep. 2007.

[45] B. Otis, Y. H. Chee, and J. Rabaey, "A 400 μW-RX, 1.6 mW-TX super-regenerative transceiver for wireless sensor networks," *in Proc. IEEE Int. Solid-State Circuits Conf.*, Feb. 2005, pp. 396–397.

[46] J. Ayers, K. Mayaram, and T. Fiez, "A 0.4 nJ/b 900 MHz CMOS BFSK super-regenerative receiver," *in Proc. Custom Integr. Circuits Conf.*, Sep. 2008, pp. 591–594.

[47] J. Ayers, K. Mayaram, and T. Fiez, "An ultralow-power receiver for wireless sensor networks," *IEEE J. Solid-State Circuits, vol. 45*, no. 9, pp. 1759–1769, Sep. 2010.

[48] P.E. Thoppay, C. Dehollain, M.M. Green, M.J. Declercq, "A 0.24-nJ/bit Super-Regenerative Pulsed UWB Receiver in 0.18-μm CMOS," *IEEE J. Solid-State Circuits, vol. 46*, no. 11, pp. 2623-2634, Nov. 2011.

[49] F.X. Moncunill-Geniz, P. Pala-Schonwalder, C. Dehollain, N. Joehl, and M. Declercq, "An 11-Mb/s 2.1-mW Synchronous Superregenerative Receiver at 2.4 GHz," *IEEE Trans. Microw. Theory Tech., vol. 5*, no. , pp. 355-1362, June 2007.

[50] K. Kim, J. Song, S. Nam, "Super-regenerative receiver for capsule endoscopy

application using digital counter," *Microwave Conference Proceedings (APMC), 2011 Asia-Pacific*, pp.1382-1385, 5-8 Dec. 2011.

[51] J. Ryu, M. Kim, J. Lee, B. Kim, M. Lee, S. Nam, "Low Power OOK Transmitter for Wireless Capsule Endoscope," *Microwave Symposium, 2007. IEEE/MTT-S International, vol., no.*, pp.855-858, 3-8 June 2007.

[52] K. Kim *et al.*, "A design of a high-speed and high-efficiency capsule endoscopy system," *IEEE Trans. Biomed. Eng., vol. 59*, no. 4, pp.1005-1011, Apr. 2012.

[53] Y. H. Chee et al., "A 46% efficient 0.8dBm transmitter for wireless sensor networks," *in Symp. VLSI Circuits Dig.*, 2006, pp.43-44.

[54] J. Jung et al., "22-pJ/bit energy-efficient 2.4-GHz implantable OOK transmitter for wireless biotelemetry systems: In vitro experiments using rat skin-mimic," *IEEE Trans. Microw. Theory Tech., vol. 58*, no. 12, pp. 4102–4111, Dec. 2010.

[55] J. Choi, K. Kim, and S. Nam, "A low power CMOS chirp-spread-spectrum OOK transmitter for in-body communication", *in Symp. Asian-Pacific EMC Dig.*, 2011.

[56] J. Choi, J. Chang, and S. Nam, "Design of wideband/high efficiency CMOS power amplifier for low power application," *in Symp. Korea-Japan Microw. Dig.*, 2011, pp. 70-73.

[57] S. C. Cripps, *RF Power Amplifiers for Wireless Communications*, 2nded. Boston, MA: Artech House, 2006.

[58] Q. Tang, S. Gupta, and L. Schwiebert, "BER performance analysis of an on-off keying based minimum energy coding for energy constrained wireless sensor applications," *in Proc. IEEE ICC*, 2005, vol. 4, pp.2734–2738.

초 록

본 논문에서는 인체 내외 통신을 위한 의료용 송수신기에서 발생하는 문제점을 인식하고 이를 해결하기 위한 방법을 제시 하였다. 인체는 높은 유전율과 도전율을 가지는 인체의 전기적 특성으로 인해 상당한 전파 손실을 가지고 있다. 이 때문에, 인체내외 통신에 사용되는 장치는 높은 sensitivity를 가져야 하고, 제한된 배터리 동작으로 인해 저전력 특성이 요구된다. 또한, 이 문제는 앞으로 이동성 기기와의 통합을 고려한다면, 인체내외 통신 장치 모두를 위해 해결해야만 한다. 동시에, 인공 안구나 다중 채널 방식의 뇌전도 센서와 같은 특정 분야에서는 장치의 높은 데이터 속도 또한 요구한다. 그래서, 인체내외 통신용 의료센서를 위해 장치의 전력소모와 데이터 전송 속도 향상은 필수적인 일이다. 인체내외 통신용 의료센서의 성능 향상을 위한 몇 가지 방법들을 본 논문에서 소개 한다.

먼저, 인체내외 통신용 주파수 선정을 위해 인체의 전파 손실을 계산하였다. 기존의 MICS 대역이나 FCC에 의해 할당 받은 주파수 대역은, 대역폭이 너무 좁거나, 인체 내에서 손실이 큰 주파수이다. 이 때문에, Friss의 공식을 이용하여, 체내외 통신을 위한 최적의 주파수를 찾고, 이를 활용하여 link budget을 계산하였다. 이로부터 캡슐용 내시경용 시스템을 설계하여, 인체 등가 매질과 돼지의 뱃속에서의 동작을 확인하여, 선정된 주파수의 타당성을 검증 하였다.

두 번째로, 저전력을 특성을 가지는 DSQL을 이용한 SRR 구조를 제안하였다. 제안된 구조의 DSQL은 기존 수신기의 포락선 검파기를 대신하여, 전체 전력을 최소화 시킨다. 또한 기존 다른 SRR과 달리 추가적인 CLOK이 필요하지 않다. 때문에 고속 동작에 유리하고, 저전력 특성을 가진다. 측정된 결과는 제안된 수신기가 저전력이고, 높은 전송속도를 필요로 하는 의료용 체내외 통신용 수신기로 적합함을 검증 하였다.

마지막으로, 저전력이면서 높은 전송속도를 가지는 CRCC PA 구조를 제안 하였다. 일반적으로 저전력용 PA는 구현가능성에 관한 이슈가 있고, 이것은 PA의 최적의 출력 임피던스가 너무 커서 안테나 단과의 매칭이 어렵기 때문이다. 이 문제 때문에, 일반적인 PA 구조로는 최대의 효율을 얻는 것이 어렵다. 게다가 일반적인 PA의 출력 대역폭은, 높은 임피던스 변환 율 때문에, 너무 좁다. CRCC 구조는 이러한 문제를, PA의 출력과 안테나의 입력 임피던스들의 변환율을 감소 시킴으로써, 해결 한다. CRCC PA 구조를 채택한 송신기를 설계하고 측정된 결과로부터 그 성능을 검증 하였다.

주요어: 고속 동작, 고효율, 슈퍼 리제네러티브, OOK 변조, 의료용 삽입물, 자체 퀸츠, 저전력, 전류 재사용, 전류 합성, 캡슐 내시경용 송수신기.
학번: 2010-30975